Time's arrow in stochastic characterization and simulation of atmospheric and hydrological processes

Demetris Koutsoyiannis
Department of Water Resources and Environmental Engineering, School of Civil Engineering, National Technical University of Athens, Zographou, Greece (dk@itia.ntua.gr, http://www.itia.ntua.gr/dk)

***Hydrological Sciences Journal*; see final article in http://dx.doi.org/10.1080/02626667.2019.1600700**

Abstract Time's arrow has important philosophical, scientific and technical connotations and is closely related to randomness as well as to causality. Stochastics offers a frame to explore, characterize and simulate irreversibility in natural processes. Indicators of irreversibility are different if we study a single process alone, or more processes simultaneously. In the former case, description of irreversibility requires at least third-order properties, while in the latter lagged second-order properties may suffice to reveal causal relations. Several examined data sets indicate that in atmospheric processes irreversibility is negligible at hydrologically relevant time scales, but may appear at the finest scales. However, the irreversibility of streamflow is marked for scales of several days and this highlights the need to reproduce it in flood simulations. For this reason, two methods of generating time series with irreversibility are developed, from which one, based on an asymmetric moving average scheme, proves to be satisfactory.

Keywords Time's arrow; Irreversibility; Causation; Chance; Randomness; Stochastic simulation

1 Introduction

Yesterday all my troubles seemed so far away.
Now it looks as though they're here to stay.
Oh, I believe in yesterday.

Paul McCartney

Time irreversibility in physics has a long history, going back to 1807, when Fourier established the basis for the modern theory of heat conduction (published later; Fourier 1822). His equations, unlike those of Newtonian mechanics, were not symmetric with respect to past and future directions of time. Thomson and Maxwell followed in the same direction, and Clausius (1850, 1854, 1865) laid the foundation for the second law of thermodynamics by examining the relation between heat transfer and work, introduced the concept (and the term) of *entropy* and connected time irreversibility with the second law. Boltzmann (1877) explained the concept of entropy in probability theoretic context, and penetrated into the concept of irreversibility, on which he had a productive debate with Planck (Hollinger and Zenzen 1985). By the end of the

19th century, the study of the laws of time irreversible processes had become popular (e.g., Natanson, 1896); however, it included obscure and circular elements which in several cases remain until the present day (e.g. the classical definition of entropy is applicable in a reversible process, which in turn is one in which the definition holds; Koutsoyiannis 2011).

The concept (and the term) of "time's arrow" was developed by Eddington (1928) to describe time directionality, which can be determined by studying the organization of atoms, molecules and bodies. He stated "*I shall use the phrase 'time's arrow' to express this one-way property of time which has no analogue in space. It is a singularly interesting property from a philosophical standpoint. We must note that: (1) It is vividly recognized by consciousness. (2) It is equally insisted on by our reasoning faculty, which tells us that a reversal of the arrow would render the external world nonsensical. (3) It makes no appearance in physical science except in the study of organization of a number of individuals. Here the arrow indicates the direction of progressive increase of the random element.*"

Time asymmetry is closely related to causality, which presupposes irreversibility. Thus, "*no causal process (i.e., such that of two consecutive phases, one is always the cause of the other) can be reversible*", while "*according to the causal theory of time, two events are simultaneous by definition if there can be no causal action between them*" (Heller 1983; see also Kline 1980). In probabilistic definitions of causality, time asymmetry is determinant. For instance, Suppes (1970) defines causation thus: "*An event* $B_{t'}$ [occurring at time t'] *is a prima facie cause of the event* A_t *if and only if (i)* $t' < t$, *(ii)* $P(B_{t'}) > 0$, *(iii)* $P(A_t|B_{t'}) > P(A_t)$." Also, Granger's (1980) first axiom in defining causality reads "*The past and present may cause the future, but the future cannot.*"

In the modern deterministic framework of dynamical systems, time reversibility and irreversibility can be understood through the following concepts (Lasota and Mackey 1994):

- A *dynamical law* S_t maps a system's state y at time $t = 0$ into new states $S_t(y)$ as time t changes, i.e., $y(t) = S_t(y(0))$.
- A *dynamical system* is, by definition, time invertible (reversible): $S_t(S_{t'}(y)) = S_{t+t'}(y)$ for $t, t' \in R$ (positive or negative), so that $S_t(S_{-t}(y)) = y$.
- A *semidynamical system* is, by definition, noninvertible (irreversible) in time: the relationship $S_t(S_{t'}(y)) = S_{t+t'}(y)$ holds only for $t, t' \in R^+$ (nonnegative), so that $S_t(S_{-t}(y)) \neq y$.

In this framework, the sequence of a system's states y as time t changes is known as a trajectory $y(t)$. However, a deterministic system description in terms of trajectories is ineffective and not far-reaching. Prigogine and Stengers (1997) remark that "*a trajectory is time reversible, and thus allows no distinction between future and past*", and (quoting Poincaré) "*explaining irreversibility in terms of trajectories that are time-reversible processes, however numerous, appears to be a purely logical error*". They appeal to abandon the trajectory description and state: "*we need a statistical description to formulate dynamics in situations where we expect irreversible processes and therefore an increase in entropy. Such situations, after all, are what we see in the world around us. Indeterminism, as conceived by Whitehead, Bergson, and Popper, now appears in*

physics." In the same line of thought, the replacement of trajectories with "flow tubes" probabilistically defined was suggested (Koutsoyiannis 2010), while this idea was explored in hydrological modelling (Montanari and Koutsoyiannis 2012).

Once we introduce probability in a system's representation, materialized in terms of a time varying probability density function of the system state, we move from a deterministic to a stochastic description. The latter is far richer: for example, we can define and study the system's entropy, which in modern terms is a purely probabilistic concept. Thus, in a dynamical (time reversible) system the entropy is constant (Mackey, 2003, p. 31), while in a semidynamical (time irreversible) system the entropy is non-decreasing reaching a limit (maximum) as $t \to \infty$ (Mackey, 2003, p. 30).

At this point it is useful to mention the so-called *God theorem* (Mackey, 2003, p. 111) which states that every continuous trajectory $x(t)$ in a space X is the trace (projection) of a single dynamical system $S_t(y)$ operating in a higher dimensional phase space Y. We then understand that, as elementary physical laws are time symmetric, the entropy increase is adherent to macroscopization of our description: in a detailed (high-dimensional) system description (Y), the entropy should be constant (time reversibility), but in a macroscopic (lower-dimensional) description (X) it may increase in time (time irreversibility). This is consistent with Eddington's view: "*Physical processes at the microscopic level are believed to be either entirely or mostly time-symmetric: if the direction of time were to reverse, the theoretical statements that describe them would remain true. Yet at the macroscopic level it often appears that this is not the case: there is an obvious direction (or flow) of time.*" In this respect, the notion of causality also presupposes macroscopization of the description and thus cannot be captured by the Newtonian or other time symmetric equations.

Having entered the world of stochastics, we can formulate a simpler definition of time reversibility using the concept of a stochastic process and bypassing that of a dynamical or a semidynamical system. We recall that a stochastic process $\underline{x}(t)$ is a collection of (usually infinitely many) random variables $\underline{x}$ indexed by t, typically representing time. In turn, a random variable, $\underline{x}$, is an abstract mathematical entity, associated with a probability distribution function, $F(x) \coloneqq P\{\underline{x} \leq x\}$, where x is any numerical value (a regular variable), P denotes probability and the symbol "$\coloneqq$" means "is defined as". A random variable $\underline{x}$ becomes identical to a regular variable x_0 only if $F(x) = H(x - x_0)$, where H is the unit step function. The stochastic process $\underline{x}(t)$ represents the evolution of the system over time, while a trajectory $x(t)$ is a realization of $\underline{x}(t)$; if it is known at certain points t_i, it is a time series. To avoid (the common practice of) confusing a random variable with a regular variable and a stochastic process with a time series, we use a careful notation adopting the so-called Dutch convention (Hemelrijk 1966), i.e., underlining random variables and stochastic processes; regular variables such as the time t or realizations of $\underline{x}$ are denoted by non-underlined symbols.

A stochastic process $\underline{x}(t)$ at (continuous) time t, with nth order distribution function

$$F(x_1, x_2, \dots, x_n; t_1, t_2, \dots, t_n) \coloneqq P\{\underline{x}(t_1) \le x_1, \underline{x}(t_2) \le x_2, \dots, \underline{x}(t_n) \le x_n\} \quad (1)$$

is time-symmetric or time-reversible if its joint distribution does not change after reflection of time about the origin, i.e., if for any n, $t_1, t_2, \dots, t_{n-1}, t_n$,

$$F(x_1, x_2, \dots, x_n; t_1, t_2, \dots, t_n) = F(x_1, x_2, \dots, x_n; -t_1, -t_2, \dots, -t_n) \quad (2)$$

The definition in (2) is adapted from Weiss (1975). Assuming that the process $\underline{x}(t)$ is stationary and that times are equidistant, i.e. $t_i - t_{i-1} = D$, and shifting the time by $\tau = 2t_1 + (n-1)D$, we get

$$F(x_1, x_2, \dots, x_{n-1}, x_n; t_1, t_2, \dots, t_{n-1}, t_n) = F(x_1, x_2, \dots, x_{n-1}, x_n; t_n, t_{n-1}, \dots, t_2, t_1) \quad (3)$$

This is a generalization for continuous time of the definition given for a coarse-grained process in discrete time by Porporato et al. (2007), while it is practically the same as in Lawrance (1991). We stress the fact (neglected in many papers) that (3) cannot be valid for arbitrary t_i, but only for equidistant ones; in contrast, (2) is a more general definition valid always. A process that is not time-reversible is called time-asymmetric, time-irreversible or time-directional. For brevity, in the next part of this paper we will drop the identifier "time" from the terms (a)symmetric, (ir)reversible and directional.

Lawrance (1991) has investigated the relationship of stationarity and reversibility, showing that if (3) holds then the process is stationary. We recall that stationary is a stochastic process whose distribution is invariant to a shift of time, so that for any n, $t_1, t_2, \dots, t_{n-1}, t_n$, and c,

$$F(x_1, x_2, \dots, x_n; t_1, t_2, \dots, t_n) = F(x_1, x_2, \dots, x_n; t_1 + c, t_2 + c, \dots, t_n + c) \quad (4)$$

Weiss (1975) showed that if the process $\underline{x}(t)$ is Gaussian (i.e., all its finite dimensional distributions are multivariate normal) then it is reversible; this means that a directional process cannot be Gaussian. He also showed that a discrete-time autoregressive moving-average (ARMA) process is reversible if and only if it is Gaussian and extended this result for continuous-time Markov processes. As noted by Lawrance (1991), "*The implications* [of Weiss's result] *are far reaching: stationary series which show evidence of directionality cannot be modelled by Gaussian ARMA models; they need to be modelled by non-Gaussian ARMA models or some type of non-linear model*." Later Lawrance (2001) investigated the relationship of reversibility with chaos and demonstrated that the chaotic behaviour is not always reversible, and is perhaps never so for monotonic many-branch maps.

Several characterizations and relevant diagnostic tests of (ir)reversibility have been proposed. Brillinger and Rosenblatt (1967) investigated the irreversibility on sunspot numbers, and presented a theory of high-order spectra, noting that their imaginary parts are zero for reversible processes. However, according to Lawrance (1991), checking this feature statistically cannot be fully practical. Ramsey and Rothman (1996) presented a test based on third order joint moments of consecutive terms of a time series, which is equivalent to testing the hypothesis that the marginal third moment of the differenced process is zero (see definition of the differenced process in section 2). This latter third moment, suitably standardized in the form

of a skewness coefficient, had earlier been suggested as a possibility to study the form of irreversibility by Cox (1981).

Chen et al. (2000) presented a test based on the fact that in a reversible process the expectation of the sine of the differenced process (multiplied by any number) is zero. This is equivalent to testing the hypothesis that the imaginary part of the characteristic function of the differenced process is zero and was also studied by Racine and Maasoumi (2007). Porporato et al. (2007) proposed as quantification of time asymmetry the relative entropy between the joint probability distribution of backward and forward sequences. A simpler statistic was proposed by Psaradakis (2008), who considered the probability of the differenced process being positive, as a simple measure of the deviation of the median of the differenced process from zero.

In a more recent and hydrologically relevant study, Müller et al. (2017) again used as an indicator of asymmetry the third moment of differences, but of the empirical copulas rather than of the time series. They justified the use of the third moment by noting that "*the power of three is applied to give large values more weight while preserving the sign*". Further, they performed simulations of combined sewer systems with original and time-reversed time series and found "*significant deviations of more than 10%*", noting that "*As in many rainfall generators the irreversibility is not explicitly considered, therefore, systematic deviations from reality may occur if synthetic series are applied to combined sewer systems*".

The result on the relation of Gaussian and reversible behaviours is valid for scalar (univariate) stochastic processes only. A vector (multivariate) process can be Gaussian and irreversible at the same time. As a simple example, we consider the following form of the autoregressive process AR(1) for discrete-time τ:

$$\underline{x}_\tau = a\underline{x}_{\tau-1} + \sqrt{1-a^2}\,\underline{v}_{\tau-\eta_0} \tag{5}$$

where $\eta_0 \geq 0$ is a time lag and $-1 < a < 1$. The innovations $\underline{v}_\tau$ are assumed independent Gaussian with zero mean and unit variance. Obviously the process $\underline{x}_\tau$ will be Gaussian too (with zero mean and unit variance) and thus it is reversible if viewed alone. However, it is more interesting to examine the vector process $\underline{\boldsymbol{y}}_\tau \coloneqq \left[\underline{x}_\tau, \underline{v}_\tau\right]^{\mathrm{T}}$, which is again Gaussian. Taking a single statistical characteristic, the expected value of the product of $\underline{\boldsymbol{y}}_\tau$ at two times with distance $\eta_0 + 1$, then reflecting time and finally shifting by $2\tau + \eta_0 + 1$, we obtain $\mathrm{E}\left[\underline{\boldsymbol{y}}_{-\tau}\underline{\boldsymbol{y}}_{-\tau-\eta_0-1}^{\mathrm{T}}\right] = \mathrm{E}\left[\underline{\boldsymbol{y}}_{\tau+\eta_0+1}\underline{\boldsymbol{y}}_{\tau}^{\mathrm{T}}\right] = \mathrm{E}\left[\underline{\boldsymbol{y}}_{\tau}\underline{\boldsymbol{y}}_{\tau+\eta_0+1}^{\mathrm{T}}\right]^{\mathrm{T}}$. The last quantity is different from $\mathrm{E}\left[\underline{\boldsymbol{y}}_{\tau}\underline{\boldsymbol{y}}_{\tau+\eta_0+1}^{\mathrm{T}}\right]$ because this matrix is not symmetric. Indeed, it can easily be verified by simple stochastic calculus that for any lag η,

$$\mathrm{E}\left[\underline{x}_\tau\underline{x}_{\tau-\eta}\right] = a^{|\eta|}, \qquad \mathrm{E}\left[v_\tau\underline{v}_{\tau-\eta}\right] = \begin{cases} 0, & \eta \neq 0 \\ 1, & \eta = 0 \end{cases}, \qquad \mathrm{E}\left[\underline{x}_\tau\underline{v}_{\tau-\eta}\right] = \begin{cases} 0 & \eta < \eta_0 \\ a^{n-\eta_0}\sqrt{1-a^2} & \eta \geq \eta_0 \end{cases} \tag{6}$$

and thus $\mathrm{E}\left[\underline{\boldsymbol{y}}_\tau\underline{\boldsymbol{y}}_{\tau+\eta_0+1}^{\mathrm{T}}\right] = \left[\left[a^{\eta_0+1}, a\sqrt{1-a^2}\right]^{\mathrm{T}}, [0,0]^{\mathrm{T}}\right]$, i.e., not symmetric (note that because of the zero mean and the unit variances, the expected values of the products are identical to correlation coefficients). In other words, equation (2) does not hold and, hence, the process is irreversible and at the same time Gaussian. A general result for any multivariate Gaussian linear

process has been presented by Tong and Zhang (2005) who demonstrated that such a process is reversible if and only if its autocovariance matrices are all symmetric. More complicated conditions in order for multivariate non-Gaussian linear processes to be symmetric have been studied by Chan et al. (2006). On a more theoretical basis, Georgiou and Lindquist (2014) presented an account of time reversal in bivariate stochastic models and showed that any model which consists of a linear stable dynamical system driven by an appropriate input process can be reversed in time.

Equation (5), along with time asymmetry, which is evident in $\mathrm{E}\left[\underline{x}_\tau \underline{v}_{\tau-\eta}\right]$ in equation (6), gives some grounds for a claim of a causal relationship between $\underline{v}_\tau$, the cause, and $\underline{x}_\tau$, the effect. In this simple case, because of the time independence of the succession of causes $\underline{v}_\tau$, the process $\underline{x}_\tau$ is not correlated with the future of the process $\underline{v}_\tau$ but is correlated with its past (at lags $\eta \geq \eta_0$). This is a strong indication that $\underline{x}_\tau$ is an effect caused by $\underline{v}_\tau$ and not the other way round. This example constitutes a simple case because of the zero correlation for positive lags, which makes detection of irreversibility clear, but such simplicity would not emerge if the past and future of $\underline{v}_\tau$ per se were (auto)correlated; that case will be discussed below.

Attributing causal relations to events and processes needs caution as we tend to see causality where chance rules (Mlodinow 2008). However, the above discourse points out the conditions that are necessary for causality claims about processes (rather than single events). A first, already obvious, condition is irreversibility as without it there cannot be causality. This condition alone makes the study of irreversibility important from both a philosophical and a practical point of view. A second condition is related to an antithesis of cross-correlations between the two processes for positive and negative lags, as that in equation (6); a formal criterion representing this condition will be formulated below. While here we discuss necessary conditions for causality claims, we clarify that we avoid seeking sufficient conditions, a task that would be too difficult or impossible without a generally acceptable formal definition of causality which is currently lacking.

As already discussed, irreversibility may have important implications, yet insufficient attention has been given to it in the hydrological and geophysical literature, with few exceptions such as those already cited. Several relevant questions have not been well studied or even not posed at all. Is irreversibility present in hydrological time series and, if yes, in what degree and at which time scales? How can irreversibility be detected and can this detection help determine causality relationships? Are customary stochastic simulation methods capable of reproducing irreversibility in a controlled manner? If not (which actually turns out to be the case) and if there are cases where irreversibility cannot be neglected, can we devise simulation techniques capable of dealing with irreversibility?

All these questions are addressed in this paper. In the next part of it, after reviewing the basic tools to study irreversibility in a stochastic context (section 2), we explore several data sets of atmospheric and hydrological processes, investigating possible irreversibility (section 3). This

exploration is made separately for bivariate processes, where causation is also discussed (section 3.1), and univariate ones (section 3.2). To keep the study simple, we are basing our exploration on moments of the examined processes. As explained before, in the bivariate processes irreversibility can be explored by means of joint second-order moments, while in the univariate case second-order moments do not provide useful information and at least third-order moments should be examined. Two simulation techniques capable of reproducing irreversibility are developed in section 4 for the univariate case, while multivariate simulation techniques are not dealt with in this paper.

2 Basic stochastic tools

In this section we provide a synopsis of the stochastic framework needed for the study, which includes classical concepts and some recent developments, whose details can be found in Koutsoyiannis (2010, 2016, 2017), along with some additional elements. Let $\underline{x}(t)$ be a stationary stochastic process representing the instantaneous quantity of a certain hydrological or other physical process in continuous time t. Fundamental characteristics of the marginal distribution of the instantaneous process $\underline{x}(t)$ are its mean and variance (assumed to be finite),

$$\mu \coloneqq \mathrm{E}[\underline{x}(t)], \quad \gamma_0 \coloneqq \mathrm{var}[\underline{x}(t)] \tag{7}$$

The most customary characteristics of the joint distribution of the process are its second-order characteristics:

- *Autocovariance function*, $c(h)$ for time lag h, defined as

$$c(h) \coloneqq \mathrm{cov}[x(t), x(t+h)] \tag{8}$$

- *Power spectrum* (also known as *spectral density*), $s(w)$ for frequency w, defined as the Fourier transform of the autocovariance function, i.e.,

$$s(w) \coloneqq 4\int_0^\infty c(h)\cos(2\pi w h)\,\mathrm{d}h \tag{9}$$

- *Structure function* (also known as *semivariogram* or *variogram*),

$$v(h) \coloneqq \frac{1}{2}\mathrm{var}\left[\underline{x}(t) - \underline{x}(t+h)\right] \tag{10}$$

- *Climacogram*, $\gamma(k)$, i.e., the variance of the averaged process at time scale k.

$$\gamma(k) \coloneqq \mathrm{var}\left[\frac{\underline{X}(k)}{k}\right] \tag{11}$$

where

$$\underline{X}(t) \coloneqq \int_0^t \underline{x}(\xi)\mathrm{d}\xi \tag{12}$$

is the cumulative process, which for natural processes $\underline{x}(t)$ is nonstationary with mean and variance, respectively,

$$\mathrm{E}\big[\underline{X}(t)\big] = \mu t, \qquad \Gamma(t) \coloneqq \mathrm{var}\big[\underline{X}(t)\big] = t^2\gamma(t) \tag{13}$$

- *Climacospectrum*, $\zeta(k)$, proportional to the difference of the variances of the averaged process at time scales k and $2k$,

$$\zeta(k) \coloneqq \frac{k\big(\gamma(k) - \gamma(2k)\big)}{\ln 2} \tag{14}$$

This resembles the power spectrum and combines the asymptotic behaviours of the climacogram and the structure function.

The asymptotic behaviours of these characteristics are given by log-log derivatives (LLD). Namely, for a function $f(t)$, LLD is formally expressed by:

$$f^{\#}(t) \coloneqq \frac{\mathrm{d}(\ln f(t))}{\mathrm{d}(\ln t)} = \frac{tf'(t)}{f(t)} \tag{15}$$

Specifically, the asymptotic behaviour of the second-order characteristics of a process for $k \to 0$ and $k \to \infty$ is characterized by two parameters, M and H, which are given as (Koutsoyiannis, 2017):

$$M \coloneqq \frac{v^{\#}(0)}{2} = \frac{\zeta^{\#}(0) - 1}{2}, \qquad H \coloneqq 1 + \frac{\gamma^{\#}(\infty)}{2} = \frac{\zeta^{\#}(\infty) + 1}{2} \tag{16}$$

where both are dimensionless and take on values between 0 and 1 (notice the effectiveness of the climacospectrum $\zeta(k)$ to express both asymptotic behaviours, while this is not possible for the other characteristics as $\gamma^{\#}(0) = v^{\#}(\infty) = 0$, irrespective of $\gamma(k)$). The parameter M (from Mandelbrot) characterizes the local behaviour or the smoothness (fractality) of the process, with M = 0.5, < 0.5 and > 0.5 corresponding, respectively, to a neutral (like a Markov), a rough and a smooth process. The parameter H (from Hurst) characterizes the global behaviour or persistence of the process, with H = 0.5, < 0.5 and > 0.5 corresponding, respectively, to a neutral (like a Markov or even white noise), antipersistent and persistent process. The multifractal literature typically confuses M and H (Koutsoyiannis et al. 2018) but they clearly differ (Koutsoyiannis 2017).

The cumulative process enables representation of the process in discrete time τ (denoting the continuous-time interval $[(\tau-1)D, \tau D]$, where D is a time unit) by

$$\underline{x}_\tau \coloneqq \frac{1}{D}\int_{(\tau-1)D}^{\tau D} \underline{x}(u)\mathrm{d}u = \frac{\underline{X}(\tau D) - \underline{X}\big((\tau-1)D\big)}{D} \tag{17}$$

This can readily be expanded to define a discrete time process averaged at scale $k = \kappa D$,

$$\underline{x}_\tau^{(\kappa)} \coloneqq \frac{\underline{X}(\tau\kappa D) - \underline{X}\big((\tau-1)\kappa D\big)}{\kappa D} = \frac{\underline{x}_{(\tau-1)\kappa+1} + \underline{x}_{(\tau-1)\kappa+2} + \cdots + \underline{x}_{\tau\kappa}}{\kappa} \tag{18}$$

Notice that for time-related quantities, in the above notation and in the next part of this article, we use Latin letters for dimensional quantities and Greek letters for dimensionless ones, where the latter are convenient when using the discrete-time variants of a process; specifically we use the following symbols:

- Time unit, *D.*
- Time, $t = \tau\, D$ where t is continuous time and τ discrete time.
- Time lag, $h = \eta\, D$.
- Time scale $k = \kappa\, D$.
- Frequency, $w = \omega / D$, related to time scale by $w = 1/k$, $\omega = 1/\kappa$.

We stress that all the above five second-order characteristics are transformations of one another and thus any one of them suffices to determine all five, as well as to infer the discrete-time versions of the characteristics. For example, given the climacogram $\gamma(k) = \Gamma(k)/k^2$, the autocorrelation in continuous and discrete time are respectively:

$$c(h) = \frac{1}{2}\frac{\mathrm{d}^2\big(\Gamma(h)\big)}{\mathrm{d}h^2}, \qquad c_\eta = \frac{1}{D^2}\left(\frac{\Gamma(|\eta+1|D) + \Gamma\big((|\eta-1|D\big)}{2} - \Gamma(|\eta|D)\right) \tag{19}$$

Details and the full set of transformations are given in Koutsoyiannis (2017).

To study the time asymmetry of processes we define the differenced process in discrete and continuous time, respectively, as

$$\underline{\tilde{x}}_\tau \coloneqq \underline{x}_\tau - \underline{x}_{\tau-1}, \qquad \underline{\tilde{x}}_{\tau,\eta} \coloneqq \underline{x}_\tau - \underline{x}_{\tau-\eta}, \qquad \underline{\tilde{x}}(t,D) \coloneqq \underline{x}(t) - \underline{x}(t-D) \tag{20}$$

The cumulative process of $\underline{\tilde{x}}_\tau$ for discrete time is

$$\underline{\tilde{X}}_\kappa \coloneqq \underline{\tilde{x}}_1 + \underline{\tilde{x}}_2 + \cdots + \underline{\tilde{x}}_\kappa = \underline{x}_1 - \underline{x}_0 + \underline{x}_2 - \underline{x}_1 + \cdots + \underline{x}_\kappa - \underline{x}_{\kappa-1} = \underline{x}_\kappa - \underline{x}_0 \tag{21}$$

and for continuous time,

$$\begin{aligned}\underline{\tilde{X}}(k,D) \coloneqq \int_0^k \underline{\tilde{x}}(t,D)\mathrm{d}t = \int_0^k \Big(\underline{x}(t) - \underline{x}(t-D)\Big)\mathrm{d}t = \int_0^k \underline{x}(t)\mathrm{d}t - \int_{-D}^{k-D} \underline{x}(t)\mathrm{d}t \\ = \underline{X}(k) - \underline{X}(k-D) + \underline{X}(-D)\end{aligned} \tag{22}$$

which for $k = \kappa\, D$, where κ is a positive integer, yields

$$\underline{\tilde{X}}(k,D) = D\big(\underline{x}_\kappa - \underline{x}_0\big) = D\underline{\tilde{X}}_\kappa \tag{23}$$

The averaged differenced process at discrete time scale κ is defined in a manner similar to (18):

$$\underline{\tilde{x}}_\tau^{(\kappa)} \coloneqq \frac{\underline{\tilde{X}}(\tau\kappa D) - \underline{\tilde{X}}\big((\tau-1)\kappa D\big)}{\kappa D} = \frac{\underline{\tilde{X}}_{\tau\kappa} - \underline{\tilde{X}}_{(\tau-1)\kappa}}{\kappa} = \frac{\underline{x}_{\tau\kappa} - \underline{x}_{(\tau-1)\kappa}}{\kappa} = \frac{\underline{\tilde{x}}_{\tau\kappa,\kappa}}{\kappa} \tag{24}$$

As seen in the expression of $\underline{\tilde{x}}_\tau^{(\kappa)}$, κ represents both time lag and time scale. In other words, in the case of the differenced process $\underline{\tilde{x}}_\tau$, averaging in time is practically identical to differencing $\underline{x}_\tau$ at higher time lags; we also notice that $\underline{\tilde{x}}_\tau^{(1)} \equiv \underline{\tilde{x}}_\tau \equiv \underline{\tilde{x}}_{\tau,1}$.

As explained in the Introduction, a minimal representation of time asymmetry will require the study of third moment μ_3 and the coefficient of skewness C_s of the process, original and differenced. We note that the first moment (mean) of the differenced process is always zero (provided that the original process is stationary), while the second one (variance) is always positive and thus it does not provide indications on time asymmetry. Thus, the least-order moment that can be used to detect reversibility is the third. For the original process, averaged at the integer time scale κ, the marginal third moment characteristics are:

$$\mu_3(\kappa) \coloneqq \mathrm{E}\left[\left(\underline{x}_\tau^{(\kappa)} - \mu\right)^3\right], \quad C_s(\kappa) \coloneqq \frac{\mu_3(\kappa)}{\left(\gamma(\kappa)\right)^{3/2}} \tag{25}$$

Here we have used the notation simplification $\gamma(\kappa D) = \gamma(\kappa)$ (and likewise for the third moment), which is legitimate as the climacogram of the discrete-time process takes identical values with that of the continuous-time process at the points where the former is defined (this is not the case for the autocorrelation and power spectrum and this constitutes one of the advantages of the climacogram and climacospectrum over other tools; for additional advantages see Koutsoyiannis 2016 and Dimitriadis and Koutsoyiannis 2015). Likewise, we denote the second and third moments of the averaged-differenced process (which obviously has mean zero) as

$$\tilde{\gamma}(\kappa) \coloneqq \mathrm{var}\left[\underline{\tilde{x}}_\tau^{(\kappa)}\right],\ \tilde{\Gamma}(\kappa) \coloneqq \mathrm{var}\left[\underline{\tilde{X}}_\kappa\right] = \kappa^2\tilde{\gamma}(\kappa),\ \ \tilde{\mu}_3(\kappa) \coloneqq \mathrm{E}\left[\left(\underline{\tilde{x}}_\tau^{(\kappa)}\right)^3\right],\ \ \tilde{C}_s(\kappa) \coloneqq \frac{\tilde{\mu}_3(\kappa)}{\left(\tilde{\gamma}(\kappa)\right)^{3/2}} \tag{26}$$

The second-order characteristics of the differenced processes can be fully determined from those of the original process. Specifically, from (21) we obtain

$$\mathrm{var}\left[\underline{\tilde{X}}_\kappa\right] = \mathrm{var}[\underline{x}_\kappa] + \mathrm{var}[\underline{x}_0] - 2\,\mathrm{cov}[\underline{x}_\kappa, \underline{x}_0] \tag{27}$$

which entails

$$\tilde{\Gamma}(\kappa) = 2c_0 - 2c_\kappa = 2v_\kappa, \qquad \tilde{\gamma}(\kappa) = \frac{2v_\kappa}{\kappa^2} \tag{28}$$

with c_κ and v_κ denoting the autocovariance and structure function at discrete time for lag κ. As $\kappa \to \infty$, the structure function tends to a finite value, $v_\kappa \to c_0$, and therefore the asymptotic behaviour of $\tilde{\gamma}(\kappa)$ is determined by the denominator κ^2 in (28); namely, $\tilde{\gamma}^{\#}(\kappa) = -2$, irrespective of $\gamma(\kappa)$, which means that $\underline{\tilde{x}}_\tau$ is completely antipersistent, irrespective of $\gamma(\kappa)$. The third-order characteristics of the differenced processes $(\tilde{\mu}_3(\kappa), \tilde{C}_s(\kappa))$ cannot be uniquely determined from those of the original process $(\mu_3(\kappa), C_s(\kappa))$.

We now focus our attention on bivariate processes whose study of interdependence may reveal time asymmetry and causation. While covariance and its equivalent standardized form, i.e., correlation, have been the most customary tools to characterize dependence, they are neither the only nor the most effective ones. As indicated with the concept of the climacogram, the variance of the process averaged at a specified time scale k provides a mathematically equivalent but statistically more advantageous tool than the standard autocorrelogram.

Applying the same idea to any two random variables $\underline{x}$ and $\underline{y}$ (possibly representing different physical quantities) with means μ_x and μ_y and standard deviations σ_x and σ_y, we may form a different type of a correlation coefficient and covariance, namely (Koutsoyiannis, 2018):

$$\rho_{xy} \coloneqq \operatorname{var}\left[\frac{1}{2}\left(\frac{\underline{x}}{\sigma_x}+\frac{\underline{y}}{\sigma_y}\right)\right], \qquad \sigma_{xy} \coloneqq \sigma_x\sigma_y\rho_{xy} = \operatorname{var}\left[\frac{1}{2}\left(\sqrt{\frac{\sigma_y}{\sigma_x}}\underline{x}+\sqrt{\frac{\sigma_x}{\sigma_y}}\underline{y}\right)\right] \tag{29}$$

We note that standardizing the variables $\underline{x}$ and $\underline{y}$ with their standard deviations is necessary if they represent different physical quantities, in order to make them compatible before taking the average. It is easily seen that ρ_{xy} is linearly related to the classical (Pearson) correlation coefficient, $r_{xy} \coloneqq \operatorname{cov}\left[\underline{x},\underline{y}\right]/(\sigma_x\sigma_y) = \operatorname{cov}\left[\underline{x}/\sigma_x,\underline{y}/\sigma_y\right]$, by $\rho_{xy} = (1+r_{xy})/2$. As is well known,r_{xy} lies in the interval [–1, 1] with the values –1, 0 and 1 representing completely anti-correlated, uncorrelated and completely correlated variables, respectively. Obviously, the same information as in r_{xy} is provided by ρ_{xy}, which lies in the interval [0, 1] with the values 0, 1/2, 1 representing fully anticorrelated, uncorrelated and fully correlated variables, respectively. Consequently, σ_{xy} lies in the interval $[0, \sigma_x\sigma_y]$.

Unlike r_{xy}, the notions of ρ_{xy} and σ_{xy} could be readily expanded to many variables and actually this is done with the climacogram. The latter can be further expanded to describe the dependence of different processes, replacing the concept of cross-correlogram of two stationary processes $\underline{x}(t)$ and $\underline{y}(t)$ by the *standardized cross-climacogram* (SCC) for scale k and lag h (Koutsoyiannis, 2019):

$$\begin{aligned}\rho_{xy}(k,h) &\coloneqq \operatorname{var}\left[\frac{1}{2}\left(\frac{\underline{X}(k)}{\sqrt{\Gamma_x(k)}}+\frac{\underline{Y}(k+h)-\underline{Y}(h)}{\sqrt{\Gamma_y(k)}}\right)\right]\\ &= \operatorname{var}\left[\frac{1}{2}\left(\frac{\underline{X}(k)/k}{\sqrt{\gamma_x(k)}}+\frac{\left(\underline{Y}(k+h)-\underline{Y}(h)\right)/k}{\sqrt{\gamma_y(k)}}\right)\right]\end{aligned} \tag{30}$$

and that of cross-covariance by the *cross-climacogram* (CC) and the *cumulative cross-climacogram* (CCC):

$$\gamma_{xy}(k,h) \coloneqq \rho_{xy}(k,h)\sqrt{\gamma_x(k)\gamma_y(k)}, \quad \Gamma_{xy}(k,h) \coloneqq \rho_{xy}(k,h)\sqrt{\Gamma_x(k)\Gamma_y(k)} \tag{31}$$

Interesting special cases of the cross-climacogram, including the lagged auto-climacogram are studied in Appendix A, where it is also shown that the SCC has the symmetric property

$$\rho_{xy}(k,h) = \rho_{yx}(k,-h) \tag{32}$$

Discrete-time versions of these quantities are easily derived.

Inspired by equations (5) and (6) and continuing the related discussion in the Introduction, we attempt to formalize a function that can quantify irreversibility even in cases where the cross covariance $\mathrm{E}\left[\underline{v}_\tau\underline{v}_{\tau+\eta}\right]$ is not zero. In the example of the Introduction, the difference of cross covariance for positive and negative lags, i.e., $\mathrm{E}\left[\underline{x}_\tau\underline{v}_{\tau-\eta}\right] - \mathrm{E}\left[\underline{x}_\tau\underline{v}_{\tau+\eta}\right]$ for $\eta \geq 0$, is a candidate. Some of its properties are: (a) this difference is nonzero for any lag $\eta \geq \eta_0$ and zero for $\eta < \eta_0$;

(b) if $a > 0$ (in other words, if $\underline{x}_\tau$ is positively autocorrelated), for $\eta \geq \eta_0$ it is a nonnegative decreasing function of the lag η, taking its maximum value $\sqrt{1-a^2}$ at lag $\eta = \eta_0$ (unless $\eta_0 = 0$, at which case the maximum value is $a\sqrt{1-a^2}$ at lag $\eta = 1$); (c) if $a < 0$ (in other words, if $\underline{x}_\tau$ is negatively autocorrelated at some lags) then the same conditions as in (b) will hold after multiplying the difference with the sign δ_η of $\mathrm{E}\left[\underline{x}_\tau, \underline{x}_{\tau+\eta-n_0}\right]$ (it is easily seen in equation (6) that this sign is the same as that of $\mathrm{E}\left[\underline{x}_\tau \underline{v}_{\tau-\eta}\right]$, so that, after multiplying with this sign, the latter quantity becomes consistently nonnegative).

The range of lags at which this difference is positive (here theoretically all $\eta \geq \eta_0$, even though for large η the difference decays very fast to zero) and the lag maximizing the cross-covariance and the cross-covariance difference (here $\eta = \eta_0$ for both cases) seem to be important features for causality characterization.

Generalizing, we may contend that if there is a causal relationship between $\underline{v}_\tau$, the cause, and $\underline{x}_\tau$, the effect, both assumed to have zero mean, then for $\eta > 0$,

$$\delta_\eta \mathrm{E}\left[\underline{x}_\tau\left(\underline{v}_{\tau-\eta} - \underline{v}_{\tau+\eta}\right)\right] = \delta_\eta \mathrm{E}\left[\underline{v}_\tau\left(\underline{x}_{\tau+\eta} - \underline{x}_{\tau-\eta}\right)\right] = \delta_\eta \mathrm{E}\left[\underline{v}_\tau \tilde{\underline{x}}_{\tau+\eta,2\eta}\right] > 0 \tag{33}$$

Extending this further, we can formulate a necessary condition for a causative relationship between the processes $\underline{v}_\tau$ and $\underline{x}_\tau$ based on either the SCC, $\rho_{v\tilde{x}}$, or the correlation coefficient, $r_{v\tilde{x}}$, between $\underline{v}_\tau$ and $\tilde{\underline{x}}_{\tau+\eta,2\eta}$, suitably lagged and differenced as indicated by the subscripts, i.e., for scale $\kappa = 1$,

$$\rho_{v\tilde{x}}(1,\eta) = \mathrm{var}\left[\frac{1}{2}\left(\frac{\underline{v}_\tau}{\sqrt{\gamma_v(1)}} + \frac{\delta_\eta\, \tilde{\underline{x}}_{\tau+\eta,2\eta}}{\sqrt{\mathrm{var}(\tilde{\underline{x}}_{\tau,2\eta})}}\right)\right], \qquad r_{v\tilde{x}}(1,\eta) = \mathrm{cov}\left[\frac{\underline{v}_\tau}{\sqrt{\gamma_v(1)}}, \frac{\delta_\eta\, \tilde{\underline{x}}_{\tau+\eta,2\eta}}{\sqrt{\mathrm{var}(\tilde{\underline{x}}_{\tau,2\eta})}}\right] \tag{34}$$

where

$$\begin{gathered}\delta_\eta = \mathrm{sign}\left(\mathrm{cov}\left[\underline{x}_\tau, \underline{x}_{\tau+\eta-n_0}\right]\right) = \mathrm{sign}\left(\mathrm{var}\left[\underline{x}_\tau\right] - \frac{1}{2}\mathrm{var}\left[\tilde{\underline{x}}_{\tau,\eta-n_0}\right]\right) \\ \eta_0 \coloneqq \arg\max |\rho_{vx}(1,\eta)|\end{gathered} \tag{35}$$

Hence the necessary condition sought that $\underline{v}_\tau$ is a cause of $\underline{x}_\tau$ is that

$$\rho_{v\tilde{x}}(1,\eta) > 1/2 \quad \text{or} \quad r_{v\tilde{x}}(1,\eta) > 0 \tag{36}$$

systematically for positive lags η or at least in a wide range defining the region where causality holds. Note that $(\rho_{v\tilde{x}} - 1/2)$ and $r_{v\tilde{x}}$ are odd functions of η. Quantitative characteristics of the causal relationship in a discrete-time representation at scale κ, are:

- The lag η_0 at which the SCC, $|\rho_{vx}(\kappa,\eta)|$, is maximized and the maximum value $|\rho_{vx}(\kappa,\eta_0)|$.
- The lag η_1 at which the differenced SCC, $\rho_{v\tilde{x}}(\kappa,\eta)$, is maximized and the maximum value $\rho_{v\tilde{x}}(\kappa,\eta_1)$.
- The range of lags η for which $\rho_{v\tilde{x}}(\kappa,\eta) > 1/2$.

The standard cross-covariances (or cross-correlations) could alternatively be used instead of cross-climacograms (or SCCs).

3 Exploration of atmospheric and hydrological data sets

3.1 Irreversibility in bivariate processes

The best known causal relationship in hydrology is that between rainfall and streamflow. Our exploration in this case is not aimed to discover a relationship but to see how this relationship is mapped using the stochastic tools described above.

In a case study we use rainfall and streamflow data from the database of the U.S. Geological Survey (https://nwis.waterdata.usgs.gov/md/nwis/uv/?site_no=01603000&agency_cd=USGS, retrieved: 2018-09-16) for the site USGS 01603000 North Branch Potomac River Near Cumberland, MD (39°37'18.5"N, 78°46'24.3"W, catchment area 2271 km^2). The data series are for the period 2013-10-01 to 2018-08-31 for time step of 15 min. The discharge data were converted from cubic feet per second to m^3/s and the precipitation data from inches to mm. Missing values (4% for discharge and 11% for precipitation for a total of 172 416 values) were left unfilled.

The two data series for precipitation and discharge are depicted in Figure 1(a). A close up of the data series for a six-month period shown in Figure 1(b) visually indicates the time asymmetry of the discharge process alone (rapid increases followed by milder decreases). For the precipitation process alone, as well as for the two processes taken together, there is no similar visual indication. However, the standardized cross-climacograms shown in Figure 1(c) provide clear indication of the time asymmetry of the bivariate process. For negative lags there is no correlation, i.e., $\rho \approx 0.5$, while for positive lags $\rho > 0.5$, with a maximum $\rho = 0.55$ at the scale of 15 min and at a lag of 16 h. This does not look too high and the reasons are many, e.g. (a) the point rainfall at the measurement site, which is the catchment outlet, is not faithfully representative of the real cause, which is the rainfall over the entire catchment; (b) the catchment filters and routes the rainfall process; (c) a dam upstream regulates the flow; and (d) the rainfall signal is highly varied and skewed.

We can reduce the process variance, by averaging at larger time scales. Then the correlation becomes stronger, reaching a peak of $\rho = 0.72$ for time scale of 96 h, beyond which the maximum ρ decreases. Thus, the evidence for causality becomes stronger by increasing the time scale up to a certain point. However, this is done at a cost, which is an artificial increase of the time to peak and the deformation of the cross-climacogram shape, whose positive values expand to the negative lags. The deformation is an effect of the fact that each of the two processes exhibits positive autocorrelation, as shown in the lagged auto-climacograms of Figure 1(d). Nonetheless, the entire picture provided by Figure 1 reflects well the causative relationship between precipitation and discharge.

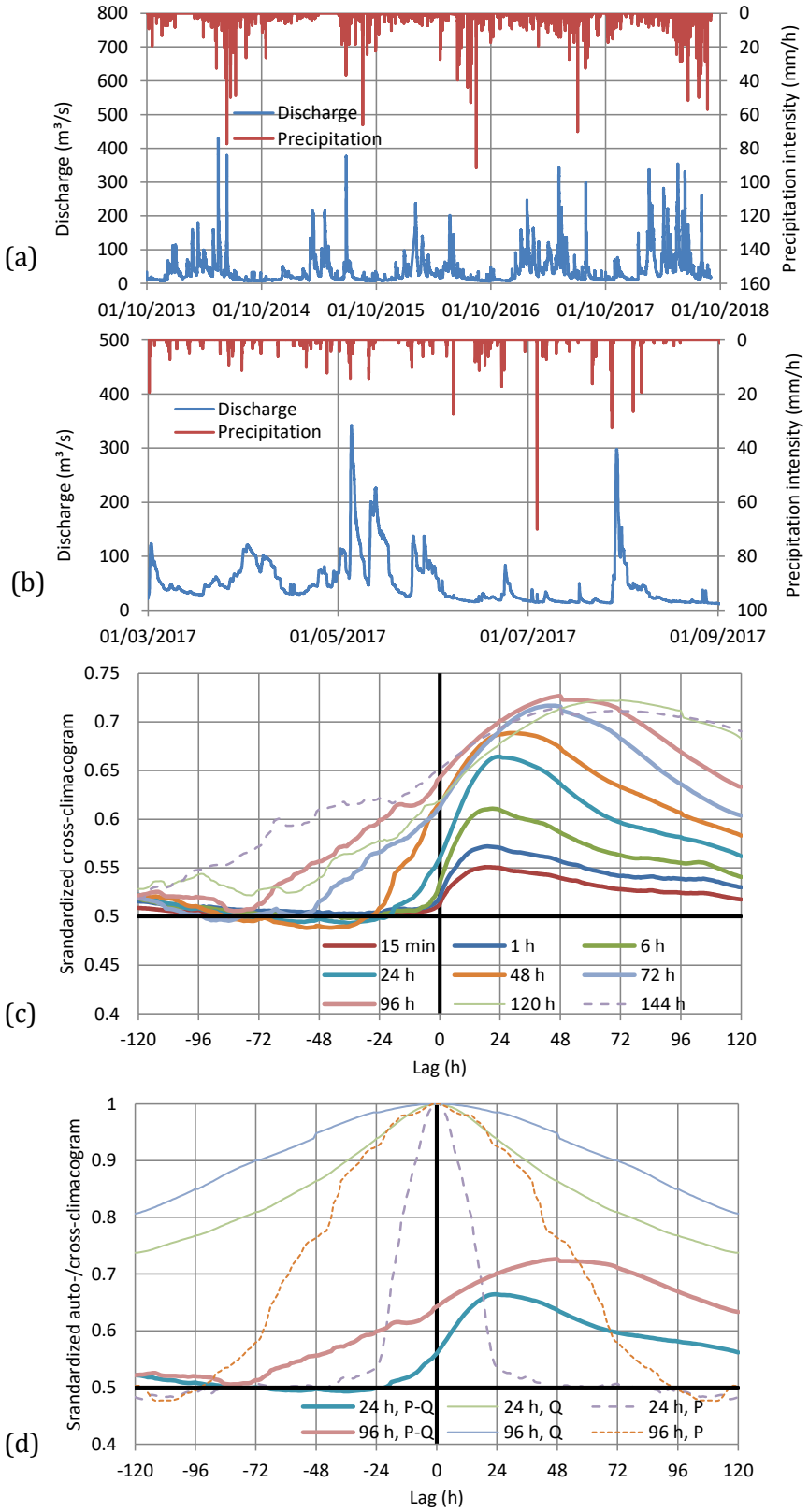

Figure 1 (a) Precipitation and discharge data series for the USGS site North Branch Potomac River Near Cumberland, MD; (b) close up of the data series for a six-month period; (c) standardized cross-climacograms for the indicated time scales and lags; (d) standardized cross-climacograms for two time scales along with the lagged auto-climacograms (P: Precipitation, Q: discharge).

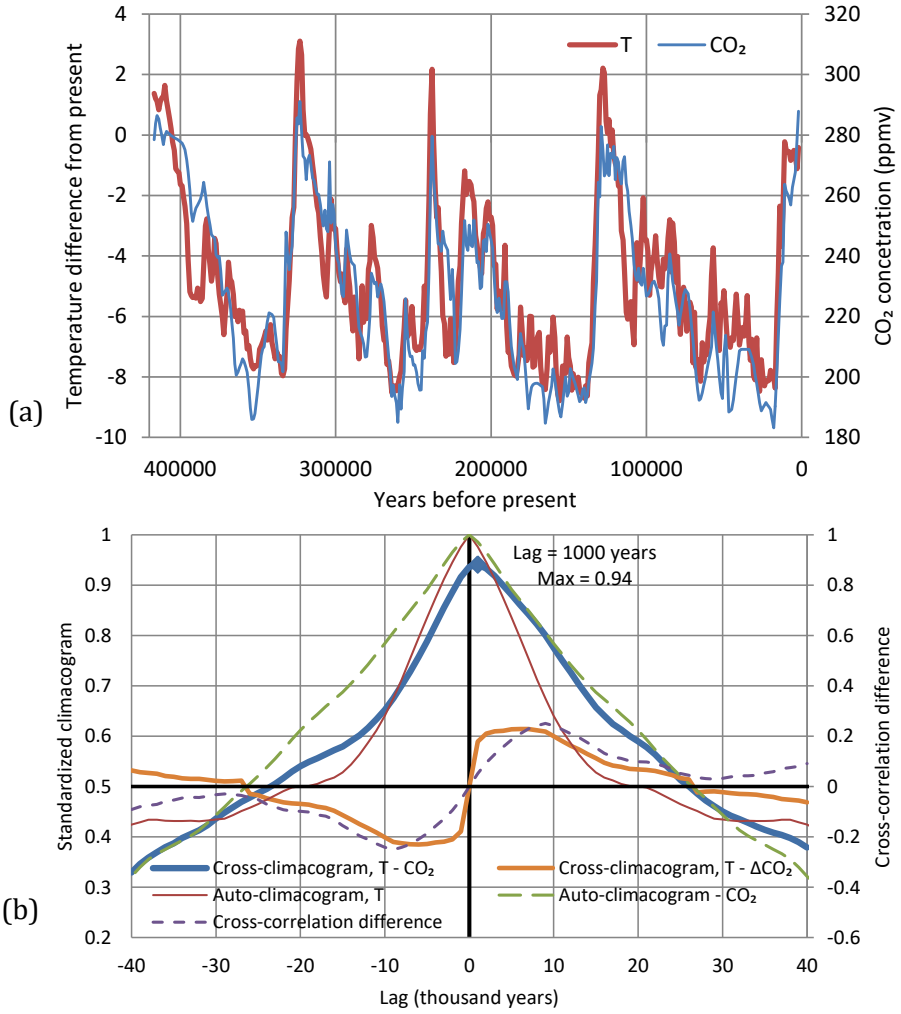

Figure 2 (a) Time series of temperature and CO_2 concentration from the Vostok ice core for time step of 1000 years; (b) standardized cross-climacograms for time scale of 1000 years along with the lagged auto-climacograms and lagged-and-differenced cross-climacogram (equation (34)); the difference of standard cross-correlation coefficients between positive and negative lags is also plotted for comparison (T: Temperature, CO_2: CO_2 concentration).

The next example is about an important yet controversial causative relation of two atmospheric processes, temperature (T) and CO_2 concentration (CO_2). To study it we use paleoclimatic data from the Vostok ice core (Jouzel et al., 1987; Petit et al. 1999). The CO_2 data were retrieved from http://cdiac.ess-dive.lbl.gov/ftp/trends/co2/vostok.icecore.co2 (accessed Sep. 2018, dated Jan. 2003) and the T data from http://cdiac.ess-dive.lbl.gov/ftp/trends/temp/vostok/vostok.1999.temp.dat (accessed Sep. 2018, dated Jan. 2000). The two data series go back to about 420 000 years before present (more precisely, before 1950) and are given for irregular time steps, which are quite different for the two series. Namely, the average time step for the T and CO_2 time series are ~128 and ~1150 years, respectively. It must be noted that the age of the gas (air bubbles) at a certain ice layer differs from the ice age; specifically, the air extracted from the ice is younger than the surrounding ice. Extensive studies to date the air with respect to ice by Barnola et al. (1991) concluded that "*the age difference between air and ice is about 6000*

years during the coldest periods instead of about 4000 years, as previously assumed". Indeed in the data provided in the above site, the difference between the ice and air age is about 6000 years for the coldest periods, decreasing to about 2000 years for the hottest periods and averaging at a difference of ~4070 years. Naturally, in our calculations for the CO_2 time series we used the air age, as given in the publicly available data series. To make calculations possible, we regularized the time reference at a constant time step of 1000 years using linear interpolation, a technique justified in Markonis and Koutsoyiannis (2013). The step of 1000 years is close to the average time step of the original CO_2 time series.

The two time series are depicted in Figure 2(a), which clearly indicates the time directionality of each of the two processes as well as the strong correlation between them. The latter is quantified by the standardized cross-climacograms shown in Figure 2(b), which provide evidence of the time asymmetry of the bivariate process. Contrary to what was observed in the previous example, there is correlation (ρ > 0.5) for both positive and negative lags, which reaches a maximum of 0.94 at a lag η_0 = 1000 years.

Generally the values of the cross-climacograms are comparable to those of the lagged auto-climacograms, shown in Figure 2(b), except in a small area near the origin. This does not help identity cause and effect. The positive lag of 1000 years in the maximum value of the SCC makes it more plausible that the temperature is the cause and the CO_2 concentration the effect. Somewhat stronger is the indication provided by the differenced cross-climacogram, estimated using (34) and also plotted in Figure 2(b) (marked as cross-climacogram T-ΔCO_2). Here the maximum value appears for lag η_1 = 5000 years and is 0.61. The graph shows that the data are consistent with the necessary condition of causality of equation (36), with T being the cause and CO_2 the effect, for all lags up to 26 000 years. The differences in standard (Pearson) correlation coefficients, also plotted in the figure, provide similar information.

Larger time scales, as in Figure 1, were also investigated but not plotted in Figure 2 to avoid an overloaded graph. At scales larger than 1000 years, the maximum value of the cross-climacogram between T and CO_2 appears at lag 0, which does not help in identifying causality. As the maximum correlation value is already very high at scale 1000 years, increasing the time scale does not make a visible difference. However, again the differenced cross climacogram (as well as the difference of cross-correlation coefficients between positive and negative lags) indicates the same pattern, positive values at positive lags and negative at negative ones.

It is quite likely that what we are observing at time scale 1000 or more years could be a SCC that has been deformed in the same way as the rainfall-streamflow relation in the previous example. That is, the time-step of 1000 years could be argued to be too long so that a more useful shape could only be captured by an analysis at finer timescales. For that reason, an analysis with time scale of 500 years was also made. This was done for half of the time series, i.e. between 119 and 325 thousand years, in which the measurements were more frequent, at an average time step of ~800 years (against ~1150 years of the entire time series). Qualitatively,

the results were the same as in 1000-year time scale, with slight increase of cross-climacogram values. Namely, the maximum value of the cross-climacogram between T and CO_2 appears again at a lag η_0 = 1000 years and it is about 0.96 (against 0.94 at the 1000-year time scale). The differenced cross-climacogram T-ΔCO_2 has a maximum value of 0.65 (against 0.61 at the 1000-year time scale) at lag η_1 = 3000 years.

The above analysis, and in particular the lag η_0 = 1000 years that maximizes the SCC and the positive values of the differenced cross-climacogram for lags up to 26 000 years, provides evidence that: (a) air temperature and CO_2 concentration are closely associated; (b) a necessary (but not sufficient) condition holds that the temperature can be the cause and the CO_2 concentration the effect; and (c) the possibility that the opposite is the case can be excluded. The positive lag, i.e. the fact that T changes first and CO_2 follows, is consistent with other studies (Soon 2007 and references therein) while the lag value of 1000 years found here is compatible with that of 800 (± 200) years found in other studies (Caillon et al., 2003); actually the coarse time resolution of the CO_2 time series does not allow distinguishing 800 from 1000 years. Whether the exact lag is 1000 or 800 years or even smaller (e.g. 400 years as in Pedro et al. 2012, a value that is not supported, though, by the present analyses, particularly that at the time step of 500 years) is irrelevant to causality identification. Equally irrelevant is whether or not the 800- or 1000-year time lag is short in comparison with the total duration of the temperature and CO_2 increases (~5000 years; Caillon et al. 2003). What actually matters for causality identification is the fact that the causality condition holds for a wide range of time lags, up to 26 000 years, and hence the time lag is positive and most likely real, as, according to Barnola et al. (1991), it cannot be explained by air dating problems.

Undoubtedly, the T-CO_2 problem is much more complex than the rainfall-runoff one, and indeed the latter cannot serve as a prototype for dealing with the former, even though in the public perception (and sometimes in the scientific community) there may be a tendency to reduce any type of causality to the simplest one (e.g. that in the example of the Introduction) or even to reverse cause and effect. For the T-CO_2 relationship one may hypothesize that there is a positive feedback loop between the two processes (change in one amplifies that in the other), with the temperature being more determinant than the CO_2 concentration. This "chicken-or-egg"[1] type of causal relationship, obviously more complex than that of exclusive roles of cause and effect, is a subject to be further explored.

3.2 Irreversibility in univariate processes

To visualize an extreme case of an irreversible process (viewed alone), in order to see how a time series from it looks, we start with a synthetic example shown in Figure 3. The time series is

[1] Even though Aristotle studied the concepts of causality and first cause, it was likely Plutarch who first posed this type of causality as a philosophical problem using the example of the chicken and the egg. He refers to it in his work *Ηθικά* (Moralia), part *Συμποσιακὰ Β* (Quaestiones convivales, B), *Πρόβλημα Γ* (Question III), "*Πότερον ἡ ἄρνις πρότερον ἢ τὸ ᾠὸν ἐγένετο*" (Which was first the bird or the egg?).

composed of 100 terms, all of which were assumed to be the control variables of a nonlinear optimization problem, solved by a commercial spreadsheet solver. The constraints were that the original series be Gaussian (quantified by a small acceptable mean-square error between the empirical and the theoretical distribution) with mean 3 and standard deviation 1, and the lag-one autocorrelation coefficient be 0.5, so that the variance of the differenced process be equal to that of the original process. The objective function to be maximized was either the coefficient of skewness of the differenced process (solution 1) or the frequency that the differenced process has a negative value (meaning that the next value of the original process would be lower than the current; solution 2). We note that in this example, because the entire setting is nonlinear, with reference to Weiss's (1975) result mentioned in the Introduction, there is no inconsistency with the constraint that the original process be Gaussian in its marginal distribution.

As seen in Figure 3, the two synthetic time series so generated are characterized by a few steep increases followed by systematic milder decreases. The differenced process is characterized by a few markedly high positive values at certain points, with all other values being negative, thus leading to a coefficient of skewness of 4.10 (or 3.34 in the case of series 2), which could obviously be (much) larger if we removed either the Gaussian constraint or the autocorrelation constraint or both.

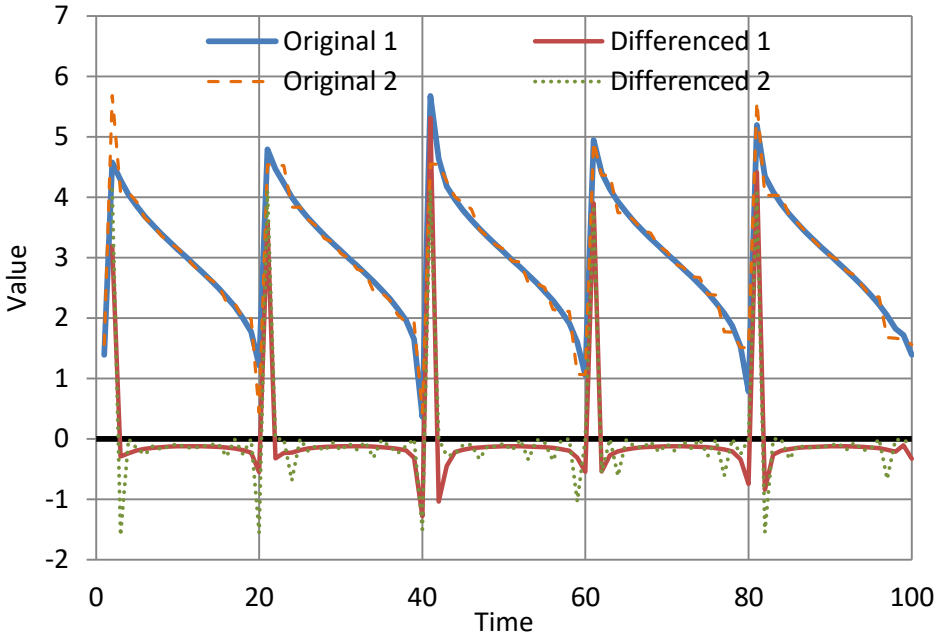

Figure 3 Plot of two synthetic time series generated by maximizing time irreversibility properties of a process restricted to be marginally Gaussian (N(3, 1)) with lag-one autocorrelation 0.5, so that the variance of the differenced process is also 1 (equal to that of the original process). Solution 1 maximizes the skewness of the differenced process. Solution 2 maximizes the frequency that the differenced process has a negative value, without taking into account the skewness. In both series the frequency that the differenced process has negative values is 0.94. The coefficients of skewness of the differenced processes for series 1 and 2 are 4.10 and 3.34, respectively.

As a general remark, before we discuss specific real-world examples, the study of time irreversibility requires estimation of third moments and skewness coefficients. It is known (e.g. Lombardo et al., 2014) that the third moment estimates are not reliable for typical sample sizes. Therefore, in all examples that follow we use samples with sizes of several thousands. If the sizes were smaller, a possibility would be to use other metrics of skewness such as the L-skewness (Hosking, 1990) or K-skewness (Koutsoyiannis, 2019) but here we preferred the simplest option, the classical skewness coefficient, accompanied by large sample sizes.

Our first real-world example for the exploration of univariate processes is a long series of nearly isotropic grid turbulence, which provides a view of the structure of a process at the finest time scales. Specifically we use grid data of turbulence from the Corrsin Wind Tunnel at a high Reynolds number (Kang et al. 2003), which were made available on the Internet by the Johns Hopkins University. This dataset consists of 40 time series with $n = 36 \times 10^6$ data points of wind velocity along the flow direction and an equal number of time series of cross-stream velocity, all measured at a sampling time interval $D = 25$ μs by X-wire probes placed downstream of the grid. Here we use part of the data, namely the series of velocity along the flow direction at the first of the probes (http://pages.jh.edu/~cmeneve1/datasets/Activegrid/M20/H1/; first column in the file), which we averaged for time scale of $D = 50$ μs, thus forming a time series with length 600 000. More data and analyses are contained in Dimitriadis and Koutsoyiannis (2018) and Koutsoyiannis (2013, 2017) in a different context, without explicitly considering the time asymmetry.

Figure 4(a) and (b) depict plots of 1/6 of the original turbulent velocity time series and the differenced one, respectively. A visual inspection of plot (a) reveals that the original process is slightly skewed (compare the very high and very low values to the mean). The same is not apparent in the differenced process. However, the coefficient of skewness of the differenced process is in fact higher (almost double, 0.353 against 0.196) than that of the original process. Further information is provided by Figure 4(c), which depicts the change with time scale of averaging of the variance and skewness of the original and the differenced process. To compile this figure we standardized the process by its standard deviation at the minimum available time scale and thus the variance of this process is 1 at this time scale. The variance decreases very slowly as the time scale increases but the variance of the differenced process is by orders of magnitude smaller. With regard to the skewness of the differenced process, the graph, in addition to the plot for the entire series, provides two more plots, one for each of the two halves of the time series, as a quick indication that the skewness estimates are reliable and their variation is systematic rather than random. We follow the same conventions also in other similar plots of the next examples.

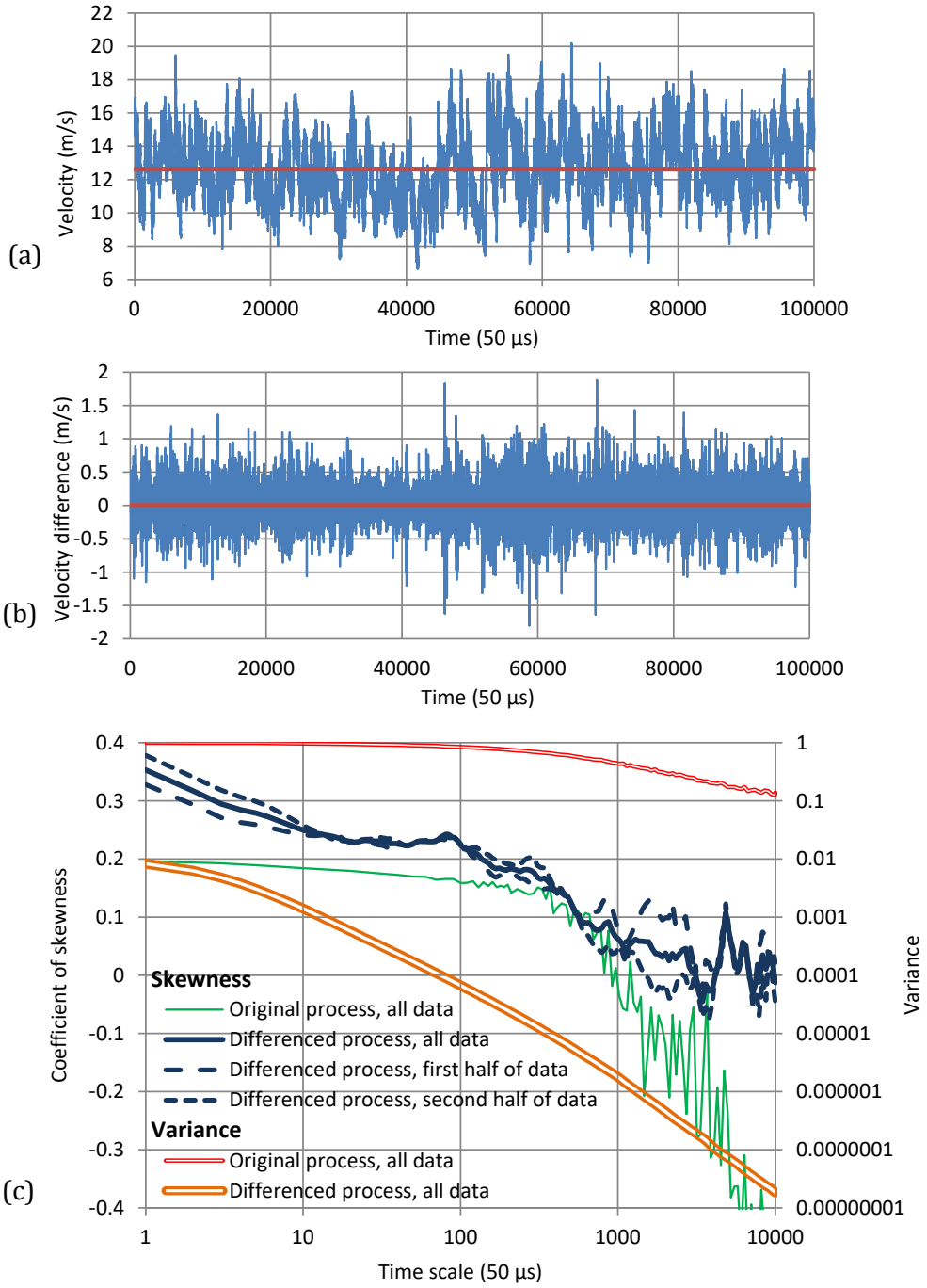

Figure 4 Plots of (a) part of the turbulent velocity time series; (b) part of the differenced time series and (c) climacograms and skewness coefficients of the original and differenced processes as functions of time scale. In (a) and (b) the means are also depicted with a thick line.

We observe in Figure 4(c) that the skewness of the original process becomes zero at a scale of about 1000 × 50 μs = 0.05 s, while the differenced process still has a positive value at this time scale and vanishes off at about twice this scale. Therefore, since a lot of studies have investigated the skewness (and intermittency) of the turbulence process, it would be equally interesting to study its time irreversibility. In any case, these may be important at the finest time scales, while as we approach the time scale of a tenth of a second, the process becomes symmetrical, both in time (reversibility) and in state (distribution function); beyond that scale the distribution of the

original process seems to become negatively skewed (which is in contrast to what we would expect from the Central Limit Theorem), yet the time symmetry, as inferred from the skewness of the differenced process, continues to hold.

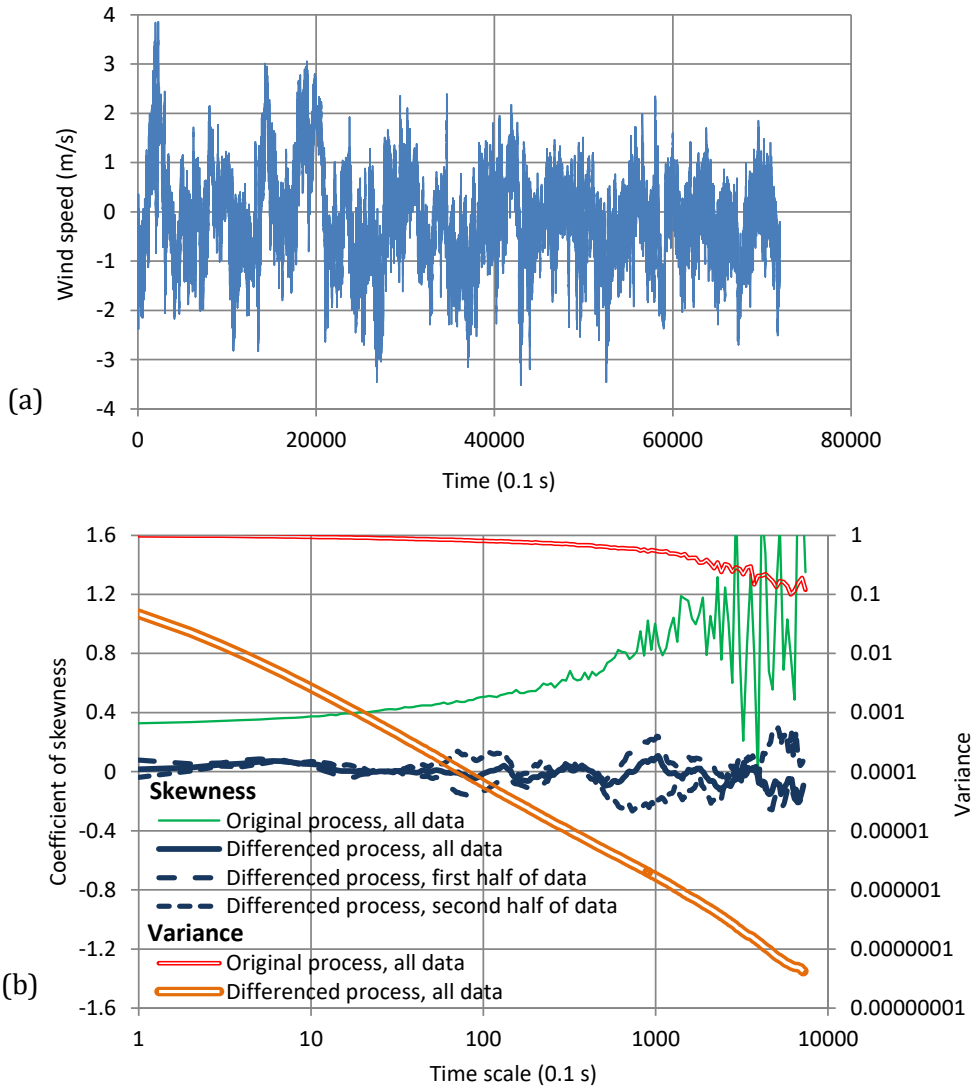

Figure 5 Plot of (a) the time series of wind speed *u* coordinate (west to east) at ABLE Beaumont site; and (b) climacograms and skewness coefficients of the original and differenced process as functions of time scale.

Next we study wind data at the much larger, yet very fine, time scale of 0.1 s. We use data recorded at a 10 Hz resolution for a period of one month by a sonic anemometer on a meteorological tower located at Beaumont KS, provided by NCAR/EOL, totalling over 25×10^6 wind speed measurements in three directions, as well as temperature measurements (Doran, 2011). Part of the data was used, namely 71 998 data values for the period starting at 1999-10-11 20:30 UTC (which is perhaps 6 h earlier in local time) and ending 2:30 h later. A plot of this part of the time series is shown in panel (a) of Figure 5, while panel (b) depicts the variation with time scale of the variance and skewness of the original and the differenced process. Neither

remarkable skewness nor time directionality are observed, a finding consistent with the previous example of turbulent velocity, as now the minimum time scale is 0.1 s.

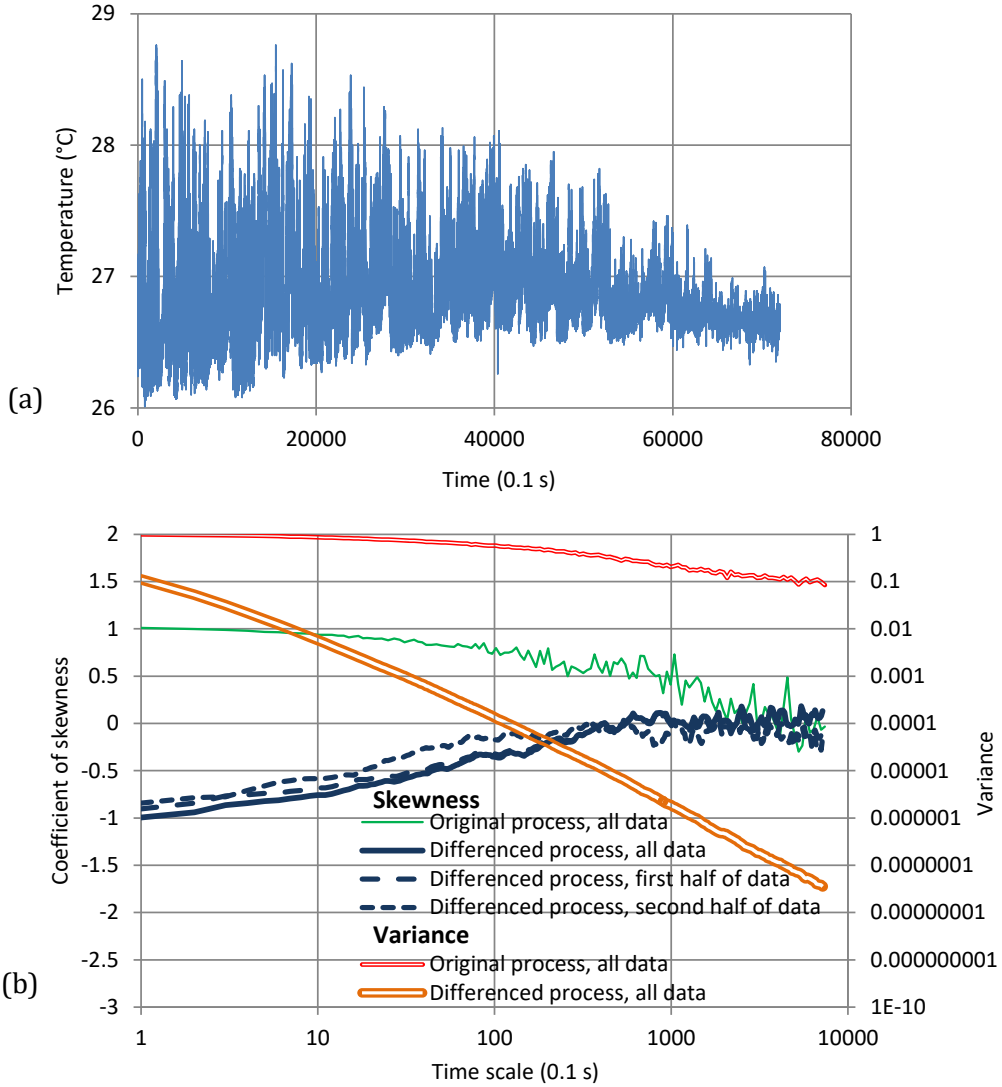

Figure 6 Plot of (a) the time series of temperature at ABLE Beaumont site; and (b) climacograms and skewness coefficients of the original and differenced process as functions of time scale.

In the next example we study the temperature measurements at the same site and the same period, from the same data set as above. The plot of Figure 6(a) shows interesting time directionality (or dependence) with decreasing variability with the increase of time. However, we may conjecture that this behaviour is local, related to the diurnal temperature cycle and would be reduced if we considered a longer period of observations for several days and if we took into account the double (daily, annual) cyclostationarity of the temperature process. Even in this part of the series both state asymmetry and time asymmetry cease at time scales of 100 s or more, as shown in Figure 6(b). It is interesting, though, that for time scales smaller than that the skewness of the original process is positive, while that of the differenced is negative.

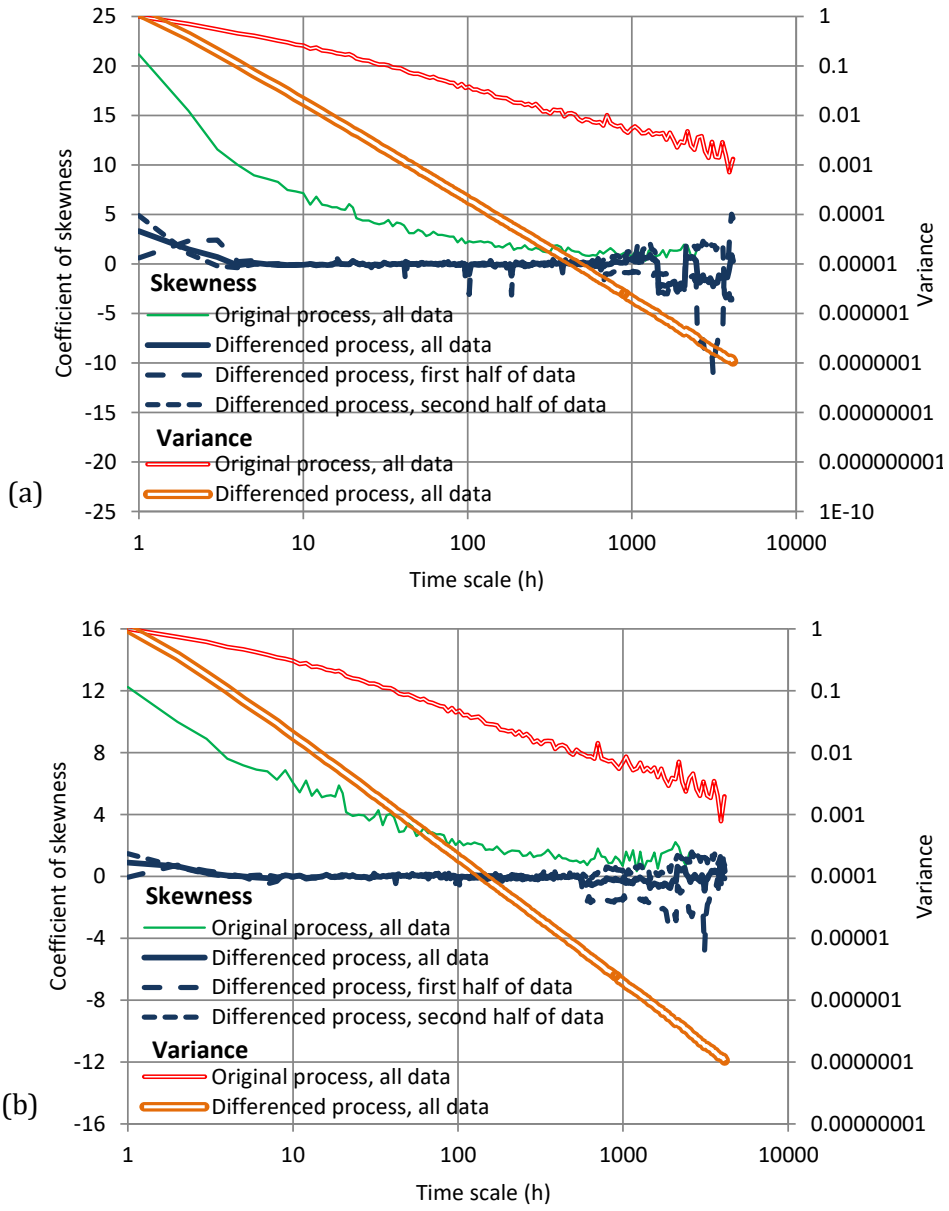

Figure 7 Climacograms and skewness coefficients of the original and differenced precipitation time series at the study site (Figure 1) as functions of time scale, (a) without transformation and (b) after standardizing for diurnal cycle.

The next example is the precipitation time series already described in section 3.1 and shown in Figure 1(a), which was measured every 15 min but here was aggregated to hourly scale. As is well-known and also confirmed in Figure 7, the variation and skewness of precipitation are very high at fine time scales. Part of the variation and also of the skewness is due to the daily and annual cycles. The effect of the former was found to be more marked than the latter and thus it was "removed" by multiplying the rainfall values by 24 different coefficients, one per hour, summing up to 1. These coefficients were found by minimizing the total variance of the transformed time series (a commercial solver was used for this task). The characteristics of the transformed time series are shown in Figure 7(b). The un-differenced transformed process still has a very high coefficients of skewness (~12), but in the differenced one the skewness and thus

the irreversibility is rather negligible. However, for time scales much lower than hourly this may not be the case and the irreversibility may be relevant for simulation of urban drainage networks, where relevant times are of the order of several minutes, rather than hours (cf. Müller et al. 2017).

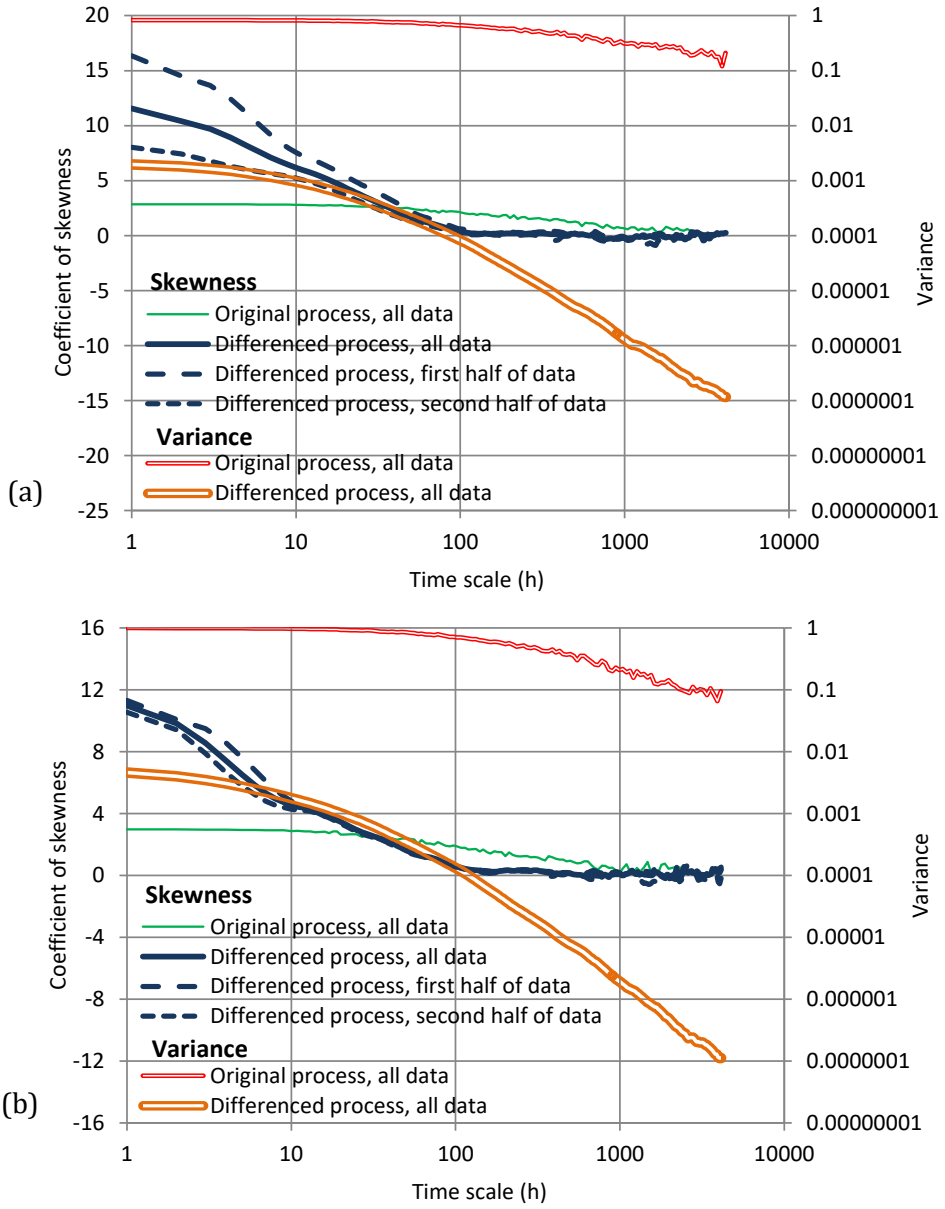

Figure 8 Climacograms and skewness coefficients of the original and differenced streamflow process at the study site as functions of time scale, (a) without transformation and (b) after standardizing for annual cycle.

The last example is the streamflow (discharge) time series already described in section 3.1 and shown in Figure 1(a), which is measured every 15 min, but here was aggregated to hourly scale. Comparing Figure 7 (rainfall) and Figure 8 (streamflow), the skewness of streamflow is much lower than that of precipitation for the original process, but the reverse happens with the differenced process, thus indicating a marked irreversibility of streamflow. Further exploration of the data indicated that, contrary to what happens with rainfall, the daily cycle has a negligible

effect on streamflow but not the annual cycle. The effect of the annual cycle was “removed” by a method similar to that described above for rainfall (i.e. multiplying the discharge values by 12 different coefficients, one per month, summing up to 1).

The characteristics of the transformed time series are shown in Figure 8(b). The skewness coefficients of the original and differenced processes after the transformation become 2.98 and 10.99, respectively, for the hourly scale, not very different from those before the transformation. The latter value indicates strong irreversibility and its attenuation is rather slow, requiring about 100 h or 4 days to vanish. This means that irreversibility is relevant for flood simulations on operational time scales, and can only be neglected for water balance and management applications that are performed on the monthly time scale.

Overall, the entire set of examples indicates that in the atmospheric processes irreversibility can be neglected at scales relevant to hydrological application, while in streamflow it is important to take into account irreversibility in flood studies. Rainfall is in between, and the irreversibility is relevant at time scales lower than hourly. Also irreversibility will be important to consider in simultaneous simulation of processes that are linked to each other by causative relations.

4 Generation of time series from univariate irreversible processes

From the above exploration, and in particular from the finding of irreversibility of streamflow series at hourly and daily scale, the need arises to devise simulation techniques that can deal with irreversibility in a controlled manner (i.e. preserving some important characteristics), of which the common simulation methods are not capable. Next we will develop two such methods based on linear filtering of non-Gaussian white noise. This general methodology, streamlined by Koutsoyiannis (2016) was extended by Dimitriadis and Koutsoyiannis (2018) and Koutsoyiannis (2019) to preserve, with explicit equations and without transformations, as many moments of the process as required. It has also been shown (Koutsoyiannis 2017) that the method can deal with any type of processes, however persistent or antipersistent, smooth or rough.

Let $\boldsymbol{c} := [c_0, c_1 \ldots, c_q]^{\mathrm{T}}$ the vector of $q + 1$ terms of the autocovariance function of a stochastic process $\underline{x}_\tau$ in discrete time τ, assumed to have zero mean. Let this be preserved by a generating scheme that filters white noise $\underline{v}_\tau$, with zero mean, unit variance and not necessarily Gaussian distribution, with a linear filter determined by a vector of $q + 1$ coefficients,

$$\boldsymbol{a} := \left[a_0, a_1, \ldots, a_q\right]^{\mathrm{T}} \tag{37}$$

The two characteristic generating schemes (Koutsoyiannis, 2000) are the symmetric moving average (SMA) scheme,

$$\underline{x}_\tau = \sum_{i=-q}^{q} a_{|i|}\underline{v}_{\tau+i} \tag{38}$$

and the asymmetric moving average (AMA) scheme,

$$\underline{x}_\tau = \sum_{i=0}^{q} a_i \underline{v}_{\tau-i} \tag{39}$$

The terms a_i are internal coefficients of the generation scheme, not model parameters to be estimated from the data. We will examine both schemes in the next subsections.

4.1 Generation method 1: Symmetric scheme for the differenced process

The SMA scheme is easier to apply as it enables an analytical solution of the coefficients $\boldsymbol{a}$. Namely, if $s_{\mathrm{d}}(\omega)$ is the power spectrum of the process in discrete time, then the Fourier transform of the sequence of coefficients $\boldsymbol{a}$, $s_{\mathrm{d}}^{a}(\omega)$, is

$$s_{\mathrm{d}}^{a}(\omega) = \sqrt{2 s_{\mathrm{d}}(\omega)} \tag{40}$$

Thus, to calculate the series of coefficients a_i we first determine $s_{\mathrm{d}}^{a}(\omega)$ and then we inverse the transform and obtain the coefficients a_i. We note that exact preservation of the second order properties of a theoretical model would in theory require an infinite number of autocovariance terms and hence an infinite number of coefficients a_i. In practice, a truncation to a specific finite q is made, resulting in a truncation error, which can be made arbitrarily small by increasing the number q. An appropriate value of q could be chosen a priori, so that the value of the last autocovariance term to be preserved, c_q, be small enough. Even if q is not chosen large enough and the truncation error is not negligible (to avoid too slow generation), it can be managed by appropriate procedures, as described in Koutsoyiannis (2016).

It can easily be verified that the SMA model always results in time symmetric processes, irrespective of the specific vector $\boldsymbol{a}$. This property of symmetric linear filters was first observed by Weiss (1975). However, if we apply the SMA scheme to the differenced process $\underline{\tilde{x}}_\tau \coloneqq \underline{x}_\tau - \underline{x}_{\tau-1}$, then we can easily reproduce its skewness (and higher order moments; see Koutsoyiannis 2019 and Dimitriadis and Koutsoyiannis 2018) and hence the characteristics of the temporal asymmetry. We recall from section 2 that $\underline{\tilde{x}}_\tau$ is completely antipersistent ($\tilde{\gamma}^{\#}(\kappa) = -2$ or $H = 0$) but this is not a problem in the generation. We also recall that the second order characteristics of $\underline{\tilde{x}}_\tau$ are determined completely from those of $\underline{x}_\tau$ by equation (28). Once we generate $\underline{\tilde{x}}_\tau$ it is easy to obtain $\underline{x}_\tau$ as the accumulation of $\underline{\tilde{x}}_\tau$. The second-order characteristics of the latter will be the correct ones, but we have no control on its skewness, its higher order moments and, eventually, its marginal distribution. In other words, with this method we can fully reproduce the marginal distribution of $\underline{\tilde{x}}_\tau$, the second-order (joint and marginal) moments of both $\underline{\tilde{x}}_\tau$ and $\underline{x}_\tau$, but not necessarily the marginal distribution of $\underline{x}_\tau$ beyond second order moments. Rather, because of the summations made to form $\underline{x}_\tau$ (the cumulative of $\underline{\tilde{x}}_\tau$) and of the Central Limit Theorem, we may expect that the marginal distribution of $\underline{x}_\tau$ will be close to normal.

Next we apply this technique to streamflow data of section 3 after their transformation to deal with seasonality. First we fit a model to the data, choosing this to be a Filtered Hurst-Kolmogorov process with a generalized Cauchy-type climacogram (FHK-C; Koutsoyiannis 2017):

$$\gamma(k) = \lambda(1 + (k/\alpha)^{2M})^{\frac{H-1}{M}} \tag{41}$$

where the dimensionless parameters M and H have been defined in equation (16), while α and λ are scale parameters with dimensions of $[t]$ and $[x^2]$, respectively. We fitted this model on the empirical estimates of the climacogram (equation (11)) and climacospectrum (equation (14)). As shown in Figure 9(a), the fitting is impressively good; the parameters are M = 0.56 (indicating a slightly smooth process), H = 0.6 (a persistent process), α = 160 h and $\lambda = \gamma(0)$ = 1.01. Additional parameters quantifying state and time asymmetry are the skewness coefficients of the original and differenced process (which as already mentioned are 2.98 and 10.99, respectively, for the hourly scale).

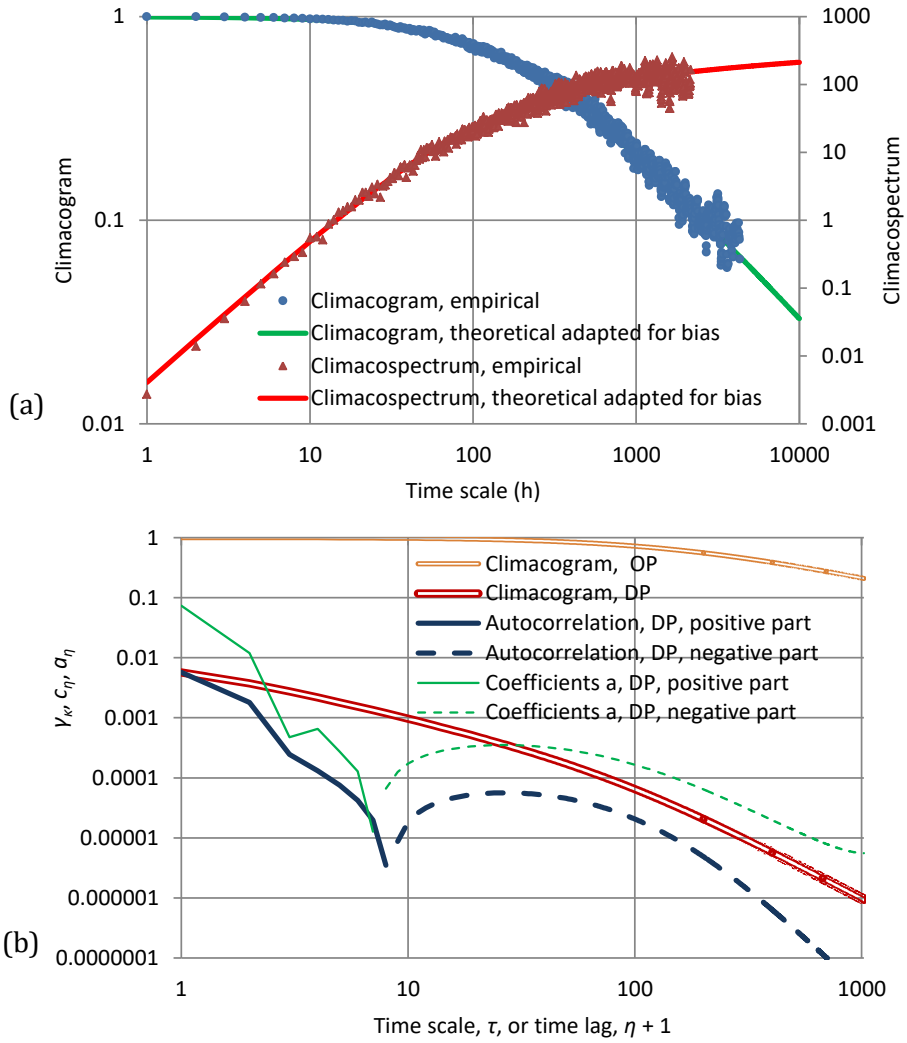

Figure 9 (a) Fit of the FHK-C model to the climacogram and climacospectrum of streamflow data of the case study (Figure 1) after their transformation to deal with seasonality and standardization to unit variance. (b) Climacogram and autocorrelation of the original and differenced process, and a values for the differenced process. (OP: original process—transformed and standardized but not differenced; DP: differenced process).

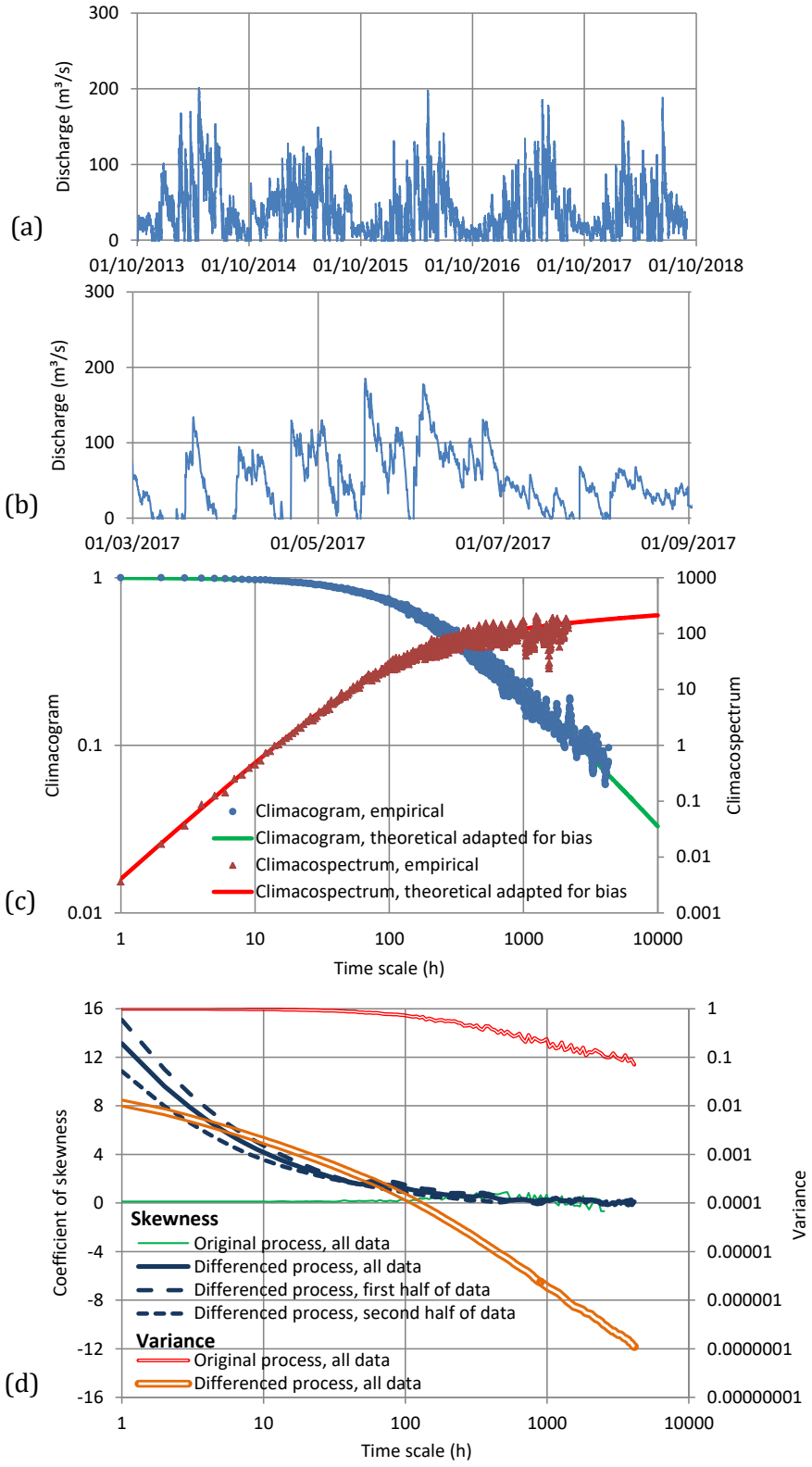

Figure 10 (a) Discharge time series generated by Method 1 (time references are arbitrary); (b) Close up of the time series for a six-month period; (c) Comparison of the climacogram and climacospectrum of the generated series with the FHK-C model; (d) Climacograms and skewness coefficients of the original and differenced time series as functions of time scale. Panels (c) and (d) refer to the series transformed for seasonality and standardized to unit variance, while (a) and (b) refer to the "naturalized" (back-transformed) series.

Once the model is fitted on the original process, the climacogram of the differenced process is determined from (28), the autocovariance function of the latter from (19) and the coefficients $\boldsymbol{a}$ from (40). For the latter we choose a number of a_i items q = 1024. All these functions are depicted in Figure 9(b). Since the differenced process $\underline{\tilde{x}}_\tau$ is completely antipersistent, the autocovariance terms and the coefficients a_i are negative except a few positive for small lags.

For the generation of the white noise the lognormal distribution was used with skewness determined so that the skewness of the differenced process be 10.99 as required. A time series with length equal to that of the real world data was then derived for the differenced process $\underline{\tilde{x}}_\tau$ using (38), and was then "naturalized" by applying the inverse seasonal transformation. Plots for the so obtained time series and their characteristics are shown in Figure 10. It is observed that the generated time series is consistent with the model and hence the original data in terms of second-order characteristics (panel (c)), but has some problems with respect to other characteristics. While both visually (panel (b)) and quantitatively (panel (d)) the irreversibility characteristics are captured, the generated series of x_τ is practically Gaussian in terms of its marginal distribution, with zero skewness and with many negative values which were truncated to zero (plot (a)).

As a result of not preserving the skewness of the original process $\underline{x}_\tau$, the behaviour with respect to maxima is not captured; rather the maxima are substantially underestimated. For all these reasons, as well its instability (sensitivity to the sequence of innovation terms and the initial value of x_0), Method 1 proves not suitable for streamflow time series. However, for a process with directionality and Gaussian marginal distribution, it could be practically suitable, The above mentioned Weiss's (1975) theoretical result says that the three behaviours, Gaussian, linear and irreversible, cannot be compatible all together. However, Method 1 does not actually generate a truly Gaussian process. Rather, it generates one with Gaussian marginal distribution, but with skewed differences (in a truly Gaussian process the differences would be Gaussian too). A Gaussian marginal distribution does not seem the case for natural hydrological processes at fine time scales, where irreversibility matters, but one could think of transforming the natural process to have Gaussian marginal distribution at a first step (as in Tsoukalas et al. 2018) and then applying Method 1 to deal with irreversibility.

4.2 Generation method 2: Asymmetric scheme for the original process

Here we develop an algorithm that can provide the coefficients a_i in an indirect, iterative manner, and without involving Fourier transforms. In method 2 the algorithm works on the original, rather than the differenced process. It is appropriate for both the SMA and the AMA schemes preserving the autocovariance and marginal distribution of the original process in both cases. In the latter case, additionally it enables the preservation of skewness of the differenced process, thus reproducing irreversibility. With either of the two schemes, once the vector of

coefficients $\boldsymbol{a}$ is specified, the autocovariance function achieved by the generating scheme, is a function of $\boldsymbol{a}$:

$$\boldsymbol{\psi} \coloneqq \left[\psi_0(\boldsymbol{a}), \psi_1(\boldsymbol{a}), \dots, \psi_q(\boldsymbol{a})\right]^{\mathrm{T}} \tag{42}$$

It can easily be verified that in both the SMA and AMA cases the autocovariance terms can be written as

$$\psi_i(\boldsymbol{a}) = \boldsymbol{A}_0^{\mathrm{T}} \boldsymbol{A}_i \tag{43}$$

where $\boldsymbol{A}_i$ is the size $(2q + 1)$ vector

$$\boldsymbol{A}_i \coloneqq \left[a_{-q+i}, \dots, a_{-1}, a_0, a_1, \dots, a_q, \underbrace{0, \dots, 0}_{i} \right]^{\mathrm{T}} \tag{44}$$

with $a_{-i} \equiv 0$ for the AMA scheme and $a_{-i} \equiv a_i$ for the SMA scheme for any $i > 0$. As a notational convention, we use regular and bold letters for scalars and vectors, respectively, with lower case for vectors with size $(q + 1)$ and upper case for those with size $(2q + 1)$.

The vector of differences between the model autocovariance vector $\boldsymbol{c}$ and that achieved by the generating scheme $\boldsymbol{\psi}$ is

$$\boldsymbol{\varepsilon}(\boldsymbol{a}) = \boldsymbol{c} - \boldsymbol{\psi}(\boldsymbol{a}) = \left[c_0 - \psi_0(\boldsymbol{a}), c_1 - \psi_1(\boldsymbol{a}), \dots, c_q - \psi_q(\boldsymbol{a})\right]^{\mathrm{T}} \tag{45}$$

and the lumped (scalar) error function is

$$e(\boldsymbol{a}) = \boldsymbol{\varepsilon}^{\mathrm{T}} \boldsymbol{\varepsilon} = (c_0 - \psi_0(\boldsymbol{a}))^2 + (c_1 - \psi_1(\boldsymbol{a}))^2 + \cdots + (c_q - \psi_q(\boldsymbol{a}))^2 \tag{46}$$

We wish to find the vector $\boldsymbol{a}$ which makes $e(\boldsymbol{a}) = 0$ or, if this is not possible, which minimizes $e(\boldsymbol{a})$. We tackle this problem in an iterative manner. Starting from an arbitrary guess $\boldsymbol{a}$ in which $e(\boldsymbol{a}) = e_1$, we find an improved value $\boldsymbol{a} - \Delta\boldsymbol{a}$ in which $e(\boldsymbol{a} - \Delta\boldsymbol{a}) = e_2 < e_1$ and proceed until the improved error becomes zero or minimum. To this aim, we apply the Newton-Raphson method in a multivariate variant we develop in Appendix D.

The method requires evaluation of the gradient of the error $e(\boldsymbol{a})$. In this evaluation, it is more convenient to express the error in terms of the size $(2q + 1)$ vector:

$$\boldsymbol{E} \coloneqq \left[\varepsilon_q, \dots \varepsilon_1, 2\varepsilon_0, \varepsilon_1, \dots, \varepsilon_q\right]^{\mathrm{T}} \tag{47}$$

(Notice the factor 2 in ε_0). Specifically, as can be easily verified, the error can be expressed as

$$e(\boldsymbol{a}) = \boldsymbol{\varepsilon}^{\mathrm{T}} \boldsymbol{\varepsilon} = \frac{1}{2} \boldsymbol{E}^{\mathrm{T}} \boldsymbol{E} - \varepsilon_0^2 \tag{48}$$

and, as shown in Appendix B, its gradient is

$$\nabla e(\boldsymbol{a}) = -2\left[\boldsymbol{E}^{\mathrm{T}} \boldsymbol{A}_0, k\boldsymbol{E}^{\mathrm{T}} \boldsymbol{A}_1, \dots, k\boldsymbol{E}^{\mathrm{T}} \boldsymbol{A}_q\right]^{\mathrm{T}} \tag{49}$$

where $k = 1$ for the AMA and $k = 2$ for the SMA.

When we are interested in time asymmetry we need also to preserve, as a minimum, the ratios of the skewness coefficients of $\underline{x}$ to those of the white noise $\underline{v}$. By preserving these ratios, if we also preserve the skewness of the original process (by appropriate choice of that of the

white noise), then we will have preserved the skewness of the differenced process. Namely, we need to preserve the ratios λ and $\tilde{\lambda}$ where:

$$\frac{\mathrm{E}\left[\underline{x}_i^3\right]}{\mathrm{E}\left[\underline{x}_i^2\right]^{3/2}} =: \lambda\, \mathrm{E}\left[\underline{v}_i^3\right], \qquad \frac{\mathrm{E}\left[\left(\underline{x}_i - \underline{x}_{i-1}\right)^3\right]}{\mathrm{E}\left[\left(\underline{x}_i - \underline{x}_{i-1}\right)^2\right]^{3/2}} =: \tilde{\lambda}\, \mathrm{E}\left[\underline{v}_i^3\right] \tag{50}$$

The third moment of $\underline{v}$, $\mathrm{E}\left[\underline{v}_i^3\right]$, is numerically equal to its skewness as by definition $\mathrm{E}\left[\underline{v}_i^2\right] = 1$. The third moment of the process achieved by the generating scheme, divided by $\mathrm{E}\left[\underline{v}_i^3\right]$, is

$$\theta(\boldsymbol{a}) = a_0^3 + a_1^3 + \cdots + a_q^3 = \boldsymbol{a}^{\mathrm{T}}\boldsymbol{a}^{(2)} \tag{51}$$

where $\boldsymbol{a}^{(2)}$ is the vector whose elements are the squares of $\boldsymbol{a}$. Likewise, the third moment of differences of consecutive $\underline{x}$, divided by $\mathrm{E}\left[\underline{v}^3\right]$, is

$$\tilde{\theta}(\boldsymbol{a}) = a_0^3 + (a_1 - a_0)^3 + \cdots + \left(a_q - a_{q-1}\right)^3 + \left(-a_q\right)^3 = \mathbf{Da}_0^{\mathrm{T}}\mathbf{Da}_0^{(2)} \tag{52}$$

where $\mathbf{Da}_i$ denotes a size $(q + 2)$ vector defined as

$$\mathbf{Da}_i := \left[\mathrm{Da}_i, \mathrm{Da}_{i+1}, \ldots, \mathrm{Da}_{i+q}, \mathrm{Da}_{i+q+1}\right]^{\mathrm{T}}, \qquad \mathrm{Da}_i := a_i - a_{i-1} \tag{53}$$

whereas $\mathbf{Da}_i^{(2)}$ is $\mathbf{Da}_i$ with squared elements, while coefficients a_i for $i < 0$ or $i > q$ are zero.

The variances achieved by the generating scheme are

$$\mathrm{E}\left[\underline{x}_i^2\right] = \psi_0(\boldsymbol{a}), \qquad \mathrm{E}\left[\left(\underline{x}_i - \underline{x}_{i-1}\right)^2\right] = 2\left(\psi_0(\boldsymbol{a}) - \psi_1(\boldsymbol{a})\right) \tag{54}$$

The errors and the squared errors (all scalars in this case) are

$$\varepsilon_{\mathrm{s}}(\boldsymbol{a}) := \lambda - \frac{\theta(\boldsymbol{a})}{\psi_0(\boldsymbol{a})^{3/2}}, \qquad e_{\mathrm{s}}(\boldsymbol{a}) = \varepsilon_{\mathrm{s}}(\boldsymbol{a})^2 \tag{55}$$

$$\tilde{\varepsilon}_{\mathrm{s}}(\boldsymbol{a}) := \tilde{\lambda} - \frac{1}{2^{3/2}} \frac{\tilde{\theta}(\boldsymbol{a})}{\left(\psi_0(\boldsymbol{a}) - \psi_1(\boldsymbol{a})\right)^{3/2}}, \qquad \tilde{e}_s(\boldsymbol{a}) = \tilde{\varepsilon}_{\mathrm{s}}(\boldsymbol{a})^2 \tag{56}$$

and, as shown in Appendix C, their gradients are

$$\nabla e_{\mathrm{s}}(\boldsymbol{a}) = -\frac{6\varepsilon_{\mathrm{s}}(\boldsymbol{a})}{\psi_0(\boldsymbol{a})^{3/2}}\left(\boldsymbol{a}^{(2)} - \frac{\theta(\boldsymbol{a})}{\psi_0(\boldsymbol{a})}\boldsymbol{a}\right) \tag{57}$$

$$\nabla \tilde{e}_{\mathrm{s}}(\boldsymbol{a}) = \frac{-3\tilde{\varepsilon}_{\mathrm{s}}(\boldsymbol{a})}{\sqrt{2}\left(\psi_0(\boldsymbol{a}) - \psi_1(\boldsymbol{a})\right)^{3/2}}\left(\mathbf{Da}_0^{(2)} - \mathbf{Da}_1^{(2)} - \frac{\tilde{\theta}(\boldsymbol{a})}{2\left(\psi_0(\boldsymbol{a}) - \psi_1(\boldsymbol{a})\right)}\left(\mathbf{Da}_0 - \mathbf{Da}_1\right)\right) \tag{58}$$

Both $\varepsilon_{\mathrm{s}}(\boldsymbol{a})$ and $\tilde{\varepsilon}_{\mathrm{s}}(\boldsymbol{a})$ should be added to $e(\boldsymbol{a})$ of equation (48) to obtain the total error. Likewise, both $\nabla e_{\mathrm{s}}(\boldsymbol{a})$ and $\nabla \tilde{e}_{\mathrm{s}}(\boldsymbol{a})$ should be added to $\nabla e(\boldsymbol{a})$ of equation (49) to determine the total gradient. Once these are determined for an initial guess of $\boldsymbol{a}$, the improvement $\Delta\boldsymbol{a}$ is

$$\Delta\boldsymbol{a} = m\frac{e(\boldsymbol{a})}{\nabla e(\boldsymbol{a})^{\mathrm{T}}\nabla e(\boldsymbol{a})}\nabla e(\boldsymbol{a}) \tag{59}$$

where the coefficient m is determined in each iteration step as detailed in Appendix D.

It is useful to know for the solution algorithm that the theoretically achieved λ and $\tilde{\lambda}$ have lower and upper limits, which are –1 and 1. These are precise for λ and correspond to the case where all $a_i = 0$, except a nonzero a_0; the limits –1 and 1 correspond to $a_0 < 0$ and $a_0 > 0$, respectively. The precise limits of $\tilde{\lambda}$ are $\pm q/\sqrt{(q+1)(q+2)}$ (apparently, tending to ±1 for large q) and correspond to the case where all but one Da_i are equal to each other. More precisely, the negative limit corresponds to a linear arrangement of a_i determined by $a_i = \sqrt{3}(i+1)/\sqrt{(q+1)(q+2)(q+3/2)}$ and the positive limit corresponds to the time reversed arrangement. The proof is omitted. Furthermore, the ratio $\tilde{\lambda}/\lambda$ cannot be arbitrarily high; an investigation showed that its upper limit is about $0.9\sqrt{q}$. In practice, the values of λ and $\tilde{\lambda}$ to be achieved should be chosen at a good distance from the theoretical limits. This is made possible by choosing a relatively high value of $\mathrm{E}\left[\underline{v}_i^3\right]$ (see eqn. (50)) or a large q if the ratio $\tilde{\lambda}/\lambda$ is high.

This method has several advantages: (a) its applicability is very broad as it works for both the SMA and the AMA scheme and in the latter case, additionally to preserving the autocovariance function, can host constraints related (but not limited) to the preservation of third moments; (b) it avoids Fourier transforms and its application is easy—e.g., it can run in a spreadsheet application without programming; (c) it is reliable as it even gives approximations if the requirements are infeasible—e.g. for non-positive definite autocorrelation sequences; (d) it is fast—particularly in the SMA case it is rapid and, provided that a good initial guess is found with the technique described in Appendix E, just one iteration usually suffices; and (e) it is computationally economic as only a few vectors, and not matrices, are needed to be stored in the computer memory (or spreadsheet). The disadvantage is that it is iterative and numerical rather than analytical.

For the application of the method with the streamflow time series we used the same model as in Method 1 with q = 1024 again, but here we directly modelled the original process, while from the differenced process we used only its skewness (10.99). The coefficients $\boldsymbol{a}$ determined after convergence of the iterative method are shown in Figure 11, along with the climacogram and the autocorrelation function of the original process.

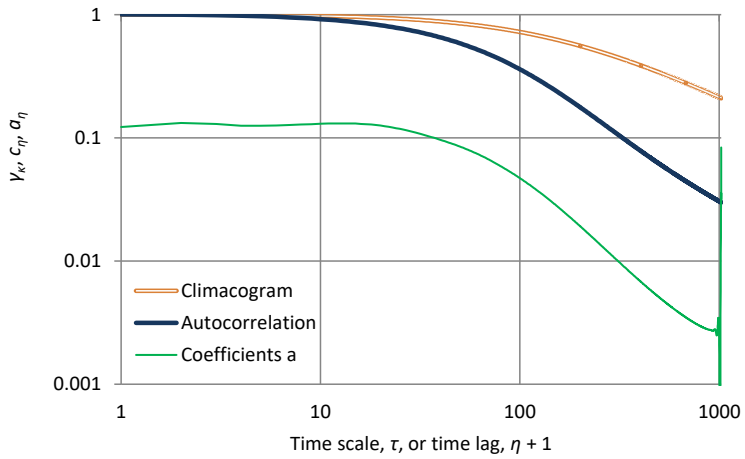

Figure 11 Climacogram, autocorrelation and a values of the original process for Method 2.

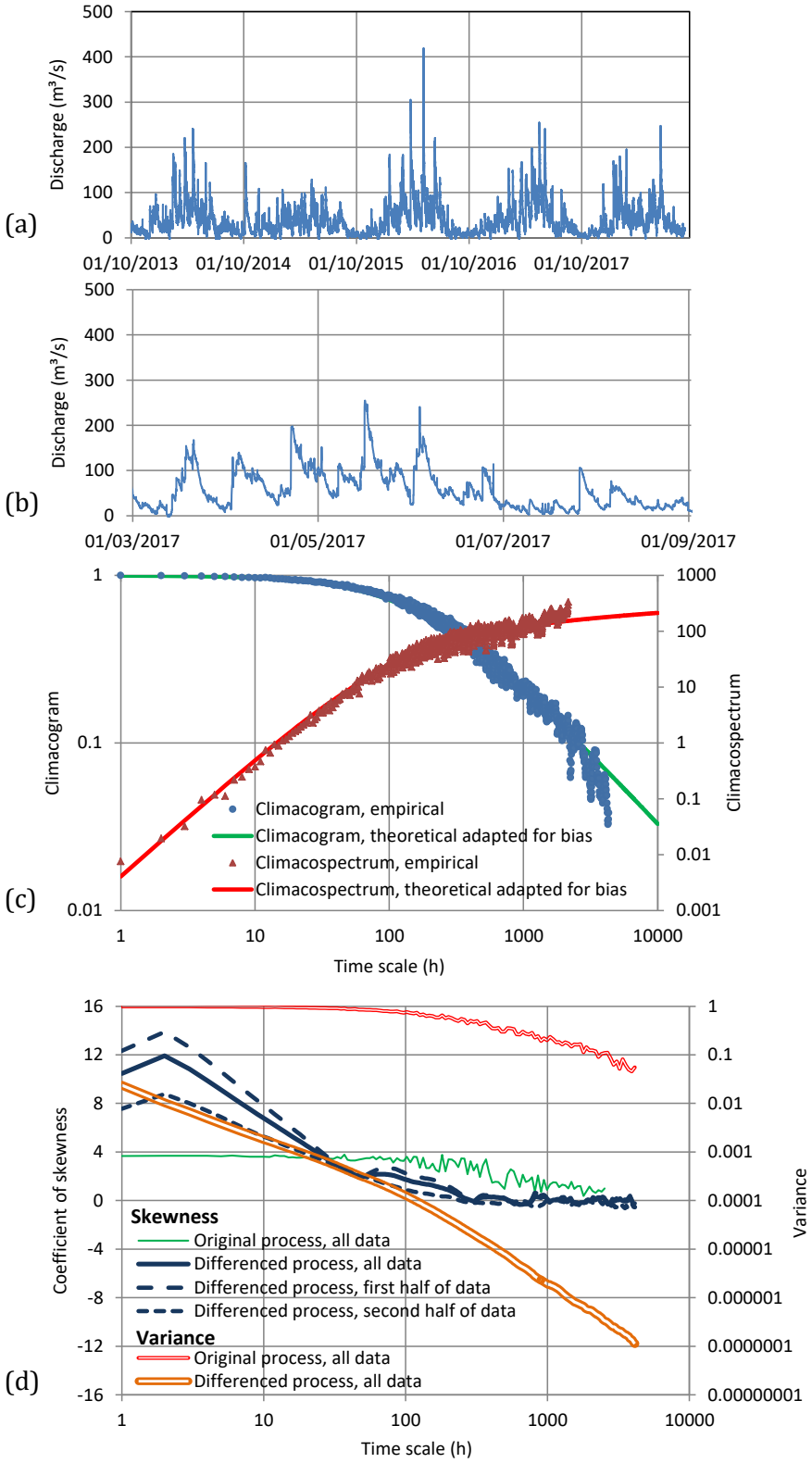

Figure 12 (a) Discharge time series generated by Method 2 (time references are arbitrary); (b) Close up of the time series for a six-month period; (c) Comparison with the FHK-C model of the climacogram and climacospectrum of the generated series; (d) Climacograms and skewness coefficients of the original and differenced time series as functions of time scale. Panels (c) and (d) refer to the series transformed for seasonality and standardized to unit variance, while (a) and (b) refer to the "naturalized" (back-transformed) series.

Again we used lognormal white noise with skewness determined so that the skewness of the original process be 2.98 as required. A time series with length equal to that of the real world data was then derived for the original process $\underline{x}_\tau$ using (39), and was then "naturalized" by applying the inverse seasonal transformation. Plots for the generated time series and their characteristics are shown in Figure 12. It is observed that the generated time series is consistent with the model and hence the original data in terms of all important statistics, marginal as well as related to time irreversibility. Therefore, Method 2 seems suitable for simulation of streamflow time series even at fine time scales.

5 Conclusions

Time's arrow has important philosophical, scientific and technical connotations and is closely related to randomness. Time asymmetry is also closely related to causality, which presupposes irreversibility. Stochastics offers a frame to explore, detect, analyse, characterize and simulate irreversibility in natural processes.

Indicators of irreversibility are different if we study a single process alone, or more processes simultaneously. In the first case, irreversibility cannot be reflected in the second-order stochastic characteristics of the process, which are by definition time symmetrical. Therefore we need to study third-order properties as a minimum. In the case of two or more processes, irreversibility can be studied in terms of lagged second-order properties and this study may reveal causal relations.

In the case of a single process, a convenient index of irreversibility is the skewness of the time differenced process, which is also related to the skewness of the marginal distribution. For theoretical reasons (cf. Central Limit Theorem), skewness vanishes off for large time scales and thus irreversibility of this type can appear in the finest time scales only. On the contrary, in bivariate or multivariate processes, irreversibility can appear at any time scale.

The example time series examined here indicate that atmospheric processes, such as wind, temperature and rainfall, do not exhibit marked irreversibility at hydrologically relevant time scales, even though for very fine scales irreversibility seems to exist. However, the irreversibility of streamflow is marked for scales of several days and this highlights the need to reproduce it in flood simulations.

For this reason, two methods of generating time series with irreversibility are developed, one of which, based on an asymmetric moving average (AMA) scheme, proves to be satisfactory for streamflow simulation. The same method can be used more generally in stochastic simulation problems, even in the case of reversibility and even for the symmetric moving average (SMA) scheme.

Appendix A – Special cases of the cross-climacogram

1. It is easily shown that the cross-climacogram has a symmetry with respect to the variables x and y. Applying the definition of the cumulative process (equation (12)), $\rho_{xy}(k,h)$ is written:

$$\rho_{xy}(k,h) = \text{var}\left[\frac{\int_0^k \underline{x}(\xi)\mathrm{d}\xi}{2\sqrt{\gamma_x(k)}} + \frac{\int_h^{k+h} \underline{y}(\xi)\mathrm{d}\xi}{2\sqrt{\gamma_y(k)}}\right] \tag{A1}$$

   Setting $\zeta = \xi - h$ we get

$$\rho_{xy}(k,h) = \text{var}\left[\frac{\int_{-h}^{k-h} \underline{x}(\xi)\mathrm{d}\xi}{2\sqrt{\gamma_x(k)}} + \frac{\int_0^k \underline{y}(\xi)\mathrm{d}\xi}{2\sqrt{\gamma_y(k)}}\right] = \text{var}\left[\frac{\underline{X}(k-h) - \underline{X}(-h)}{2\sqrt{\gamma_x(k)}} + \frac{\underline{Y}(k)}{2\sqrt{\gamma_y(k)}}\right] \tag{A2}$$

   (note that $\underline{X}(0) = \underline{Y}(0) \equiv 0$), and finally we find

$$\rho_{xy}(k,h) = \rho_{yx}(k,-h) \tag{A3}$$

2. For $k \to 0$, we get the instantaneous SCC and CC; in this case $\underline{X}(k)/k \to \underline{x}(0)$ and $\left(\underline{Y}(k+h) - \underline{Y}(h)\right)/k \to \underline{y}(h)$, and thus from equation (30) and (31) we get

$$\rho_{xy}(0,h) = \text{var}\left[\frac{1}{2}\left(\frac{\underline{x}(0)}{\sqrt{\gamma_x(0)}} + \frac{\underline{y}(h)}{\sqrt{\gamma_y(0)}}\right)\right], \qquad \gamma_{xy}(0,h) \coloneqq \rho_{xy}(0,h)\sqrt{\gamma_x(0)\gamma_y(0)} \tag{A4}$$

   We note though that the instantaneous process is hardly measured and thus it is the cross-climacogram on a finite time scale k that provides a convenient means for estimation. Another reason favouring the use of a finite time scale is that some models, such as the Hurst-Kolmogorov process, entail infinite theoretical variance of the instantaneous process, which makes calculations impossible.
3. For $\underline{x} \equiv \underline{y}$ the cross-climacogram becomes the lagged auto-climacogram taking the form

$$\gamma_{xx}(k,h) = \text{var}\left[\frac{\underline{X}(k) + \underline{X}(k+h) - \underline{X}(h)}{2k}\right], \qquad \rho_{xx}(k,h) = \frac{\gamma_{xx}(k,h)}{\gamma_x(k)} \tag{A5}$$

   In this case the symmetry equation (A3) becomes

$$\rho_{xx}(k,h) = \rho_{xx}(k,-h) \tag{A6}$$

   which shows that $\gamma_{xx}(k,h)$ is an even function with respect to the lag h.
4. For $\underline{x} \equiv \underline{y}$ and $h = 0$ the cross-climacogram becomes identical to the climacogram:

$$\gamma_{xx}(k,0) = \text{var}\left[\frac{\underline{X}(k)}{k}\right] = \gamma_x(k), \qquad \rho_{xx}(k,0) = 1 \tag{A7}$$

5. For $\underline{x} \equiv \underline{y}$ and $h = k$ the cross-climacogram becomes identical to the climacogram at the double time scale:

$$\gamma_{xx}(k,k) = \text{var}\left[\frac{\underline{X}(2k)}{2k}\right] = \gamma_x(2k), \qquad \rho_{xx}(k,k) = \frac{\gamma_x(2k)}{\gamma_x(k)} \tag{A8}$$

Appendix B – Proof of equation (49)

The derivative of the error with respect to a_i is

$$\frac{\partial e(\boldsymbol{a})}{\partial a_i} = \frac{\partial \boldsymbol{\varepsilon}^{\mathrm{T}}\boldsymbol{\varepsilon}}{\partial a_i} = 2\boldsymbol{\varepsilon}^{\mathrm{T}}\frac{\partial \boldsymbol{\varepsilon}}{\partial a_i} = -2\boldsymbol{\varepsilon}^{\mathrm{T}}\frac{\partial \boldsymbol{\psi}}{\partial a_i} \tag{B1}$$

By virtue of (43), the vector of achieved autocovariances can be expressed as

$$\boldsymbol{\psi}(\boldsymbol{a})^{\mathrm{T}} = \left[\boldsymbol{A}_0^{\mathrm{T}}\boldsymbol{A}_0, \boldsymbol{A}_0^{\mathrm{T}}\boldsymbol{A}_1, \dots, \boldsymbol{A}_0^{\mathrm{T}}\boldsymbol{A}_q\right]^{\mathrm{T}} = \boldsymbol{A}_0^{\mathrm{T}}\left[\boldsymbol{A}_0, \boldsymbol{A}_1, \dots, \boldsymbol{A}_q\right] = \boldsymbol{A}_0^{\mathrm{T}}[\boldsymbol{B}] \tag{B2}$$

whereas $[\boldsymbol{B}]$ is the $(2q + 1) \times (q + 1)$ matrix

$$[\boldsymbol{B}] \coloneqq \left[\boldsymbol{A}_0, \boldsymbol{A}_1, \dots, \boldsymbol{A}_q\right] \tag{B3}$$

Thus,

$$\frac{\partial \boldsymbol{\psi}}{\partial a_i} = \frac{\partial [\boldsymbol{B}]^{\mathrm{T}}\boldsymbol{A}_0}{\partial a_i} = \frac{\partial [\boldsymbol{B}]^{\mathrm{T}}}{\partial a_i}\boldsymbol{A}_0 + [\boldsymbol{B}]^{\mathrm{T}}\frac{\partial \boldsymbol{A}_0}{\partial a_i} \tag{B4}$$

We observe that the partial derivatives of vectors on the right-hand side have only sparse items equal to 1 while all other items are zero. By inspection it can be verified that

$$-\boldsymbol{\varepsilon}^{\mathrm{T}}\frac{\partial \boldsymbol{\psi}}{\partial a_i} = -k_i\boldsymbol{E}^{\mathrm{T}}\boldsymbol{A}_i \tag{B5}$$

where $k_i = 1$ for the AMA, while for SMA $k_0 = 1, k_i = 2$ for $i > 0$.

Appendix C – Proof of equations (57) and (58)

The derivative of the errors with respect to a_i are

$$\frac{\partial e_{\mathrm{s}}(\boldsymbol{a})}{\partial a_i} = \frac{\partial \varepsilon_s^2}{\partial a_i} = 2\varepsilon_{\mathrm{s}}\frac{\partial \varepsilon_{\mathrm{s}}}{\partial a_i} = -\frac{\varepsilon_{\mathrm{s}}}{\psi_0(\boldsymbol{a})^{3/2}}\left(-\frac{3\theta(\boldsymbol{a})}{\psi_0(\boldsymbol{a})}\frac{\partial \psi_0(\boldsymbol{a})}{\partial a_i} + 2\frac{\partial \theta(\boldsymbol{a})}{\partial a_i}\right) \tag{C1}$$

and

$$\begin{aligned}\frac{\partial \tilde{e}_{\mathrm{s}}(\boldsymbol{a})}{\partial a_i} = \frac{\partial \tilde{\varepsilon}_s^2}{\partial a_i} = 2\tilde{e}_{\mathrm{s}}\frac{\partial \tilde{\varepsilon}_{\mathrm{s}}}{\partial a_i} = &-\frac{\tilde{\varepsilon}_{\mathrm{s}}}{2\sqrt{2}\left(\psi_0(\boldsymbol{a}) - \psi_1(\boldsymbol{a})\right)^{3/2}} \\ &\times\left(-\frac{3\tilde{\theta}(\boldsymbol{a})}{\psi_0(\boldsymbol{a}) - \psi_1(\boldsymbol{a})}\left(\frac{\partial \psi_1(\boldsymbol{a})}{\partial a_i} - \frac{\partial \psi_0(\boldsymbol{a})}{\partial a_i}\right) + \frac{\partial \tilde{\theta}(\boldsymbol{a})}{\partial a_i}\right)\end{aligned} \tag{C2}$$

Now the derivatives appearing in the inner parenthesis are

$$\frac{\partial \psi_0(\boldsymbol{a})}{\partial a_i} = \frac{\partial \boldsymbol{a}_0^{\mathrm{T}}\boldsymbol{a}_0}{\partial a_i} = 2a_i, \qquad \frac{\partial \psi_1(\boldsymbol{a})}{\partial a_i} = \frac{\partial \boldsymbol{a}_0^{\mathrm{T}}\boldsymbol{a}_1}{\partial a_i} = a_{i+1} + a_{i-1} \tag{C3}$$

so that

$$\frac{\partial \psi_1(\boldsymbol{a})}{\partial a_i} - \frac{\partial \psi_0(\boldsymbol{a})}{\partial a_i} = a_{i+1} + a_{i-1} - 2a_i = \mathrm{Da}_{i+1} - \mathrm{Da}_i \tag{C4}$$

The derivatives of θ and $\tilde{\theta}$ are

$$\frac{\partial\theta(\boldsymbol{a})}{\partial a_i} = 3a_i^2, \qquad \frac{\partial\tilde{\theta}(\boldsymbol{a})}{\partial a_i} = 3(a_i - a_{i-1})^2 - 3(a_{i+1} - a_i)^2 = 3\mathrm{Da}_i^2 - 3\mathrm{Da}_{i+1}^2 \tag{C5}$$

Combining these we find

$$\frac{\partial e_\mathrm{s}(\boldsymbol{a})}{\partial a_i} = -\frac{6\varepsilon_\mathrm{s}}{\psi_0(\boldsymbol{a})^{3/2}}\left(-\frac{\theta(\boldsymbol{a})}{\psi_0(\boldsymbol{a})}a_i + a_i^2\right) \tag{C6}$$

$$\frac{\partial\tilde{e}_\mathrm{s}(\boldsymbol{a})}{\partial a_i} = -\frac{3\tilde{\varepsilon}}{\sqrt{2}\big(\psi_0(\boldsymbol{a}) - \psi_1(\boldsymbol{a})\big)^{3/2}}\left(-\frac{\tilde{\theta}(\boldsymbol{a})(\mathrm{Da}_i - \mathrm{Da}_{i+1})}{2\big(\psi_0(\boldsymbol{a}) - \psi_1(\boldsymbol{a})\big)} + (\mathrm{Da}_i^2 - \mathrm{Da}_{i+1}^2)\right) \tag{C7}$$

which prove (57) and (58).

Appendix D: The Newton-Raphson method for a scalar function of a vector variable

We first refer to the fully scalar version of the method and then extend it to the case of a scalar function of a vector variable. We assume an error function $e(a)$ dependent on a scalar argument a and we wish to find the value of the argument for which $e(a) = 0$. Starting from an arbitrary guess a in which $e(a) = e_1$ we find an improved guess $a - \Delta a$ in which $e(a - \Delta a) = e_2$. The increment Δa is determined as

$$\Delta a = m\frac{e(a)}{e'(a)} \tag{D1}$$

where $e'(a)$ is the derivative of the function $e(a)$ and m is a number which in the standard Newton-Raphson method equals 1. For a faster convergence, as well as for making the method more robust in the case where $e(a)$ has no root, we can modify m by using the value $e_2 = e(a - \Delta a)$, determined for $m = 1$ and without further evaluating the derivative $e'(a - \Delta a)$. This looks particularly useful for the vector case that is developed below, as in that case, while $e(a)$ remains a scalar, $e'(a)$ becomes a vector and thus more time consuming to evaluate.

From the known points $e_1 = e(a)$, $e_2 = e(a - \Delta a)$ and the value $e'(a)$ we can fit a parabola $\hat{e}(a)$ (a second order polynomial) to approximate the function $e(a)$ and we can calculate a new Δa and hence a value of m, which corresponds to $\hat{e}(a) = 0$ or, in the case that $\hat{e}(a)$ has no root, to the minimum value of $\hat{e}(a)$. After algebraic manipulation, which is omitted here, it is seen that m is independent of $e'(a)$ and is given in terms of the value $e_1/(2e_2)$ by

$$m = \begin{cases} \dfrac{e_1}{2e_2}, & 0 \le \dfrac{e_1}{2e_2} \le 2 \\ \dfrac{e_1}{2e_2} - \mathrm{sign}\left(\dfrac{e_1}{2e_2}\right)\sqrt{\dfrac{e_1}{2e_2}\left(\dfrac{e_1}{2e_2} - 2\right)}, & \text{otherwise} \end{cases} \tag{D2}$$

The upper equation in (D2) corresponds to the case where $\hat{e}(a)$ has no root.

Now let us assume that $\boldsymbol{a} \coloneqq [a_0, a_2, \ldots, a_q]^\mathrm{T}$ is a vector variable and instead of the scalar derivative $e'(a)$ we have a vector derivative, i.e.,

$$\nabla e \coloneqq \left[\frac{\partial e}{\partial a_0}, \quad \frac{\partial e}{\partial a_1}, \ldots, \quad \frac{\partial e}{\partial a_q}\right]^{\mathrm{T}} \tag{3}$$

Using the Taylor expansion of $e(\boldsymbol{a})$ around the initial guess $\boldsymbol{a}$, we can approximate the value at $\boldsymbol{a} - \Delta\boldsymbol{a}$ as

$$e(\boldsymbol{a} - \Delta\boldsymbol{a}) \approx e(\boldsymbol{a}) - \nabla e(\boldsymbol{a})^{\mathrm{T}} \Delta\boldsymbol{a} \tag{D4}$$

As the equation

$$e(\boldsymbol{a}) - \nabla e(\boldsymbol{a})^{\mathrm{T}} \Delta\boldsymbol{a} = 0 \tag{D5}$$

is scalar, depending on a vector of unknowns, it will normally have an infinite number of solutions $\Delta\boldsymbol{a}$ and it is reasonable to seek the one with the lowest norm $\|\Delta\boldsymbol{a}\|^2$. In other words, we minimize $\|\Delta\boldsymbol{a}\|^2$ subject to the equality constraint (D5). Introducing a Lagrange multiplier ν, we minimize:

$$f(\Delta\boldsymbol{a}) \coloneqq \|\Delta\boldsymbol{a}\|^2 + \nu\big(e(\boldsymbol{a}) - \nabla e(\boldsymbol{a})^{\mathrm{T}} \Delta\boldsymbol{a}\big) \tag{D6}$$

whose derivatives with respect to Δa_i, $i = 0, \ldots, q$, are

$$\frac{\partial f(\Delta\boldsymbol{a})}{\partial \Delta a_i} = 2\Delta a_i - \nu \frac{\partial e(\boldsymbol{a})}{\partial a_i} = 0 \tag{D7}$$

This means that Δa_i shall be proportional to $\partial e(\boldsymbol{a})/\partial a_j$ or $\Delta\boldsymbol{a}$ parallel to $\nabla e(\boldsymbol{a})$. Hence (D5) becomes

$$e(\boldsymbol{a}) - (\nu/2)\nabla e(\boldsymbol{a})^{\mathrm{T}} \nabla e(\boldsymbol{a}) = 0 \tag{D8}$$

so that

$$\nu = \frac{2e(\boldsymbol{a})}{\nabla e(\boldsymbol{a})^{\mathrm{T}} \nabla e(\boldsymbol{a})} \tag{D9}$$

Notice that both the nominator and the denominator of (D9) are scalar. Combining (D7) and (D9) the solution is found to be that of equation (59), where we also inserted a multiplicative factor m as in (D1), which could again be determined from (D2). It can easily be seen that (59) reduces to (D1) if $\boldsymbol{a}$ becomes scalar. It can be also seen that equation (59) resembles that of the steepest descent method in multivariate optimization, except that the multiplier of $\nabla e(\boldsymbol{a})$ is specified rather than left to be determined by line optimization.

We clarify that (59) is evaluated for the first time with $m = 1$ thus enabling the determination of an initial $\Delta\boldsymbol{a}$ and hence e_2, from which m is determined from (D2). With this m we evaluate again equation (59) and find the final $\Delta\boldsymbol{a}$ of the current iteration, which we subtract from the initial $\boldsymbol{a}$. We replace $\boldsymbol{a}$ with $\boldsymbol{a} - \Delta\boldsymbol{a}$, and continue with a new iteration until a termination condition is satisfied. To avoid trapping in a local optimum, we make the replacement of $\boldsymbol{a}$ with $\boldsymbol{a} - \Delta\boldsymbol{a}$ even if the error is not improving. For termination we can use the condition that improvement is not possible after a number (say, 10) of consecutive iteration steps.

Appendix E: Initial guess of coefficients

From a systematic investigation of case studies, it was observed that the algorithm can perform well with an arbitrary initial guess, but its convergence can be faster if the initial guess is a good one, such as

$$a_i = \text{sign}(c_i)\,|c_i|^{\beta}, \qquad \beta = \frac{3/2 - H}{2 - 2H} \tag{E1}$$

where H is the Hurst coefficient. This ensures that the log-log slope of the series of a_i at large i will be the correct one. The series produced by (E1) is then proportionally adjusted so that the resulting $\psi_0 = \boldsymbol{A}_0^{\mathrm{T}}\boldsymbol{A}_0$ is equal to the process variance.

In particular, for the SMA case, an almost perfect initial guess can be determined by the following steps.

1. We assume that the climacogram $\boldsymbol{\gamma} := [\gamma_1, \gamma_2, \ldots, \gamma_{2q}]^{\mathrm{T}}$ is known for time scales 1 to $2q$.
2. We determine the climacospectrum $\boldsymbol{\zeta} := [\zeta_1, \zeta_2, \ldots, \zeta_q]^{\mathrm{T}}$ from
$$\zeta_\kappa := \frac{\kappa(\gamma_\kappa - \gamma_{2\kappa})}{\ln 2} \tag{E2}$$
3. We take the square root of the climacospectrum, $\zeta_\kappa^a = \sqrt{\zeta_\kappa}$ and form the vector $\boldsymbol{\zeta}^a$ which behaves like a climacospectrum of the coefficients a. This step is inspired by the fact that the squared Fourier transform of the coefficients a equals the power spectrum of the process, while at the same time the climacospectrum resembles the power spectrum (Koutsoyiannis, 2017). Note though that the algorithm proposed here does not involve Fourier transforms.
4. We calculate the "climacogram" corresponding to $\boldsymbol{\zeta}^a$ by the inverse transformation of (E2), which is (Koutsoyiannis, 2017):
$$\gamma_\kappa^a \approx \frac{(e\ln 2)\kappa + 2}{2\kappa + 2} I_\kappa^a, \qquad e = \frac{1}{1 - 2^{2H-2}}, \qquad I_\kappa = I_{\kappa+1} + \frac{\zeta_\kappa^a}{\kappa^2}, \qquad I_{q+1} = \frac{2\zeta_{q+1}^a}{(q+1)^2} \tag{E3}$$
Note that the calculation is made in reverse order of κ.
5. We determine the a values as if they were the autocorrelation coefficients making up the climacogram γ_κ^a, i.e.,
$$a_\kappa = \frac{(\kappa+1)^2\gamma_{\kappa+1}^a + (\kappa-1)^2\gamma_{\kappa-1}^a}{2} - \kappa^2\gamma_\kappa^a \tag{E4}$$

Acknowledgments. I gratefully acknowledge technical discussions with Panayiotis Dimitriadis and Theano (Any) Iliopoulou and more philosophical ones with Antonis Christofides. The detailed, penetrating and very constructive review comments by the reviewer Christian Onof, and the suggestions by the Associate Editor Krzysztof Kochanek helped improve the paper substantially. I also acknowledge the positive critique by an anonymous reviewer of the second review round.

Funding information. No funding was provided for this research.

Conflicts of interest. No conflict of interest exists.

References

Barnola, J.M., Pimienta, P., Raynaud, D. and Korotkevich, Y.S., 1991. CO2-climate relationship as deduced from the Vostok ice core: A re-examination based on new measurements and on a re-evaluation of the air dating. *Tellus B*, 43(2), 83-90.

Boltzmann, L., 1877. Über die Beziehung zwischen dem zweiten Hauptsatze der mechanischen Wärmetheorie und der Wahrscheinlichkeitsrechnung respektive den Sätzen über das Wärmegleichgewicht. Wiener Ber., 76, 373–435 (in German).

Brillinger, D.R., and Rosenblatt, M., 1967. Computation and interpretation of k-th order spectra. In *Spectral Analysis of Time Series*, Ed. B. Harris. 189-232, Wiley, New York.

Caillon, N., Severinghaus, J.P., Jouzel, J., Barnola, J.M., Kang, J. and Lipenkov, V.Y., 2003. Timing of atmospheric CO2 and Antarctic temperature changes across Termination III. *Science*, 299(5613), 1728-1731.

Chan, K.S., Ho, L.H., and Tong, H., 2006. A note on time-reversibility of multivariate linear processes. *Biometrika*, *93*(1), 221-227.

Chen, Y.T., Chou, R.Y., and Kuan, C.M., 2000. Testing time reversibility without moment restrictions. *Journal of Econometrics*, 95(1), pp.199-218.

Clausius, R., 1850. Über die bewegende Kraft der Wärme und die Gesetze, welche sich daraus für die Wärmelehre selbst ableiten lassen. *Annalen der Physik*, 79, 500–524. doi: 10.1002/andp.18501550403 (in German). English translation: Clausius, R. 1851. On the moving force of heat, and the laws regarding the nature of heat itself which are deducible therefrom. *London, Edinburgh, and Dublin Philosophical Magazine and Journal of Science*, 4, 2 (VIII), 102–119.

Clausius, R., 1854. Über eine veränderte Form des zweiten Hauptsatzes der mechanischen Wärmetheorie. *Annalen der Physik*, 481–506, doi: 10.1002/andp.18541691202 (in German). English translation: Clausius, R.,1856. On a modified form of the second fundamental theorem in the mechanical theory of heat. *London, Edinburgh, and Dublin Philosophical Magazine and Journal of Science*. 4, 2, 86.

Clausius, R., 1865. Über verschiedene für die Anwendung bequeme Formen der Hauptgleichungen der mechanischen Wärmetheorie. *Annalen der Physik und Chemie*, 125 (7), 353–400. doi: 10.1002/andp.18652010702 (in German).

Cox, D.R., 1981. Statistical analysis of time series: Some recent developments. *Scandinavian Journal of Statistics*, 8, 93-115.

Dimitriadis, P., and Koutsoyiannis, D., 2015. Climacogram versus autocovariance and power spectrum in stochastic modelling for Markovian and Hurst–Kolmogorov processes. *Stochastic Environmental Research & Risk Assessment*, 29 (6), 1649–1669, doi: 10.1007/s00477-015-1023-7.

Dimitriadis, P., and Koutsoyiannis, D., 2018. Stochastic synthesis approximating any process dependence and distribution. *Stochastic Environmental Research & Risk Assessment*, 32 (6), 1493–1515, doi: 10.1007/s00477-018-1540-2.

Doran, C., 2011. Anemometer - Sonic at ABLE Beaumont Site Data. Version 1.0. UCAR/NCAR - Earth Observing Laboratory, http://data.eol.ucar.edu/dataset/45.910. Accessed 2018-09-17.

Eddington, A., 1928. *The Nature of the Physical World*. Cambridge University Press, Cambridge, UK.

Fourier, J., 1822. *Théorie Analytique de la Chaleur*. Firmin Didot Père et Fils, Paris.

Georgiou, T.T. and Lindquist, A., 2014. On time-reversibility of linear stochastic models. *IFAC Proceedings Volumes*, 47(3), 10403-10408.

Granger, C.W., 1980. Testing for causality: a personal viewpoint. *Journal of Economic Dynamics and Control*, 2, 329-352.

Heller, M., 1983 Time, causality, and the quantum theory, *The Review of Metaphysics*, 37(2), 408–409.

Hemelrijk, J., 1966. Underlining random variables. *Statistica Neerlandica*, 20 (1), 1-7.

Hollinger, H.B. and Zenzen, M.J., 1985. *The Nature of Irreversibility: A Study of its Dynamics and Physical Origins*. D. Reidel Publishing Company, Dordrecht, Holland.

Hosking, J.R.M., 1990. L-moments: analysis and estimation of distributions using linear combinations of order statistics. *Journal of the Royal Statistical Society, Series B*, 52, 105–124.

Jouzel, J., Lorius, C., Petit, J.R., Genthon, C., Barkov, N.I., Kotlyakov, V.M., and Petrov, V.M., 1987. Vostok ice core: a continuous isotope temperature record over the last climatic cycle (160 000 years). *Nature*, 329, 403-408.

Kang, H.S., Chester, S., and Meneveau, C., 2003. Decaying turbulence in an active-grid-generated flow and comparisons with large-eddy simulation. *J. Fluid Mech.*, 480, 129–160.

Kline, A.D., 1980. Are there cases of simultaneous causation?. In *PSA: Proceedings of the Biennial Meeting of the Philosophy of Science Association*. Vol. 1980, 1, 292-301. Philosophy of Science Association.

Koutsoyiannis, D., 2000. A generalized mathematical framework for stochastic simulation and forecast of hydrologic time series. *Water Resources Research*, 36 (6), 1519–1533, doi: 10.1029/2000WR900044.

Koutsoyiannis, D., 2010. A random walk on water, *Hydrology and Earth System Sciences*, 14, 585–601, doi: 10.5194/hess-14-585-2010.

Koutsoyiannis, D., 2011. Hurst-Kolmogorov dynamics as a result of extremal entropy production. *Physica A: Statistical Mechanics and its Applications*, 390 (8), 1424–1432, doi: 10.1016/j.physa.2010.12.035.

Koutsoyiannis, D., 2013. Hydrology and change. *Hydrological Sciences Journal*, 58 (6), 1177–1197, doi: 10.1080/02626667.2013.804626.

Koutsoyiannis, D., 2016. Generic and parsimonious stochastic modelling for hydrology and beyond. *Hydrological Sciences Journal*, 61 (2), 225–244, doi: 10.1080/02626667.2015.1016950.

Koutsoyiannis, D., 2017. Entropy production in stochastics. *Entropy*, 19 (11), 581, doi: 10.3390/e19110581.

Koutsoyiannis, D., 2019. Knowable moments for high-order stochastic characterization and modelling of hydrological processes, *Hydrological Sciences Journal*, 64 (1), 19–33, doi: 10.1080/02626667.2018.1556794.

Koutsoyiannis, D., Dimitriadis, P., Lombardo, F., and Stevens, S., 2018. From fractals to stochastics: Seeking theoretical consistency in analysis of geophysical data. *Advances in Nonlinear Geosciences*, edited by A.A. Tsonis, 237–278, doi:10.1007/978-3-319-58895-7_14, Springer.

Lasota, A., and Mackey, M.C., 1994. *Chaos, Fractals and Noise*, Springer-Verlag, New York.

Lawrance, A.J., 1991. Directionality and reversibility in time series. *International Statistical Review*, 59(1) 67-79.

Lawrance, A.J., 2001. Chaos: but not in both directions!. *Statistics and Computing*, 11(3), 213-216.

Lombardo, F., Volpi, E., Koutsoyiannis, D., and Papalexiou, S.M., 2014. Just two moments! A cautionary note against use of high-order moments in multifractal models in hydrology, *Hydrology and Earth System Sciences*, 18, 243–255, doi: 10.5194/hess-18-243-2014.

Mackey, M.C., 2003. *Time's Arrow: The Origins of Thermodynamic Behavior*, Dover, Mineola, NY, USA, 175 pp.

Markonis, Y., and Koutsoyiannis, D., 2013. Climatic variability over time scales spanning nine orders of magnitude: Connecting Milankovitch cycles with Hurst–Kolmogorov dynamics. *Surveys in Geophysics*, 34 (2), 181–207, doi: 10.1007/s10712-012-9208-9.

Mlodinow, L., 2008. *The Drunkard's Walk: How Randomness Rules Our Lives*. Pantheon, New York.

Montanari, A. and Koutsoyiannis, D., 2012. A blueprint for process-based modeling of uncertain hydrological systems. *Water Resources Research*, 48, W09555, doi: 10.1029/2011WR011412.

Müller, T., Schütze, M. and Bárdossy, A., 2017. Temporal asymmetry in precipitation time series and its influence on flow simulations in combined sewer systems. *Advances in Water Resources*, 107, 56-64.

Natanson, L., 1896. On the laws of irreversible phenomena. *The London, Edinburgh, and Dublin Philosophical Magazine and Journal of Science*, 41(252), 385-406. doi: 10.1080/14786449608620860.

Pedro, J.B., Rasmussen, S.O. and van Ommen, T.D., 2012. Tightened constraints on the time-lag between Antarctic temperature and CO 2 during the last deglaciation. *Climate of the Past*, 8(4), 1213-1221.

Petit, J.R., Jouzel, J., Raynaud, D., Barkov, N.I., Barnola, J.-M., Basile, I., Bender, M., Chappellaz, J., Davis, M., Delayque, G., Delmotte, M., Kotlyakov, V.M., Legrand, M., Lipenkov, V.Y., Lorius, C., Pepin, L., Ritz, C., Saltzman, E., and Stievenard. M., 1999. Climate and atmospheric history of the past 420,000 years from the Vostok ice core, Antarctica. *Nature*, 399, 429-436.

Porporato, A., Rigby, J.R., and Daly, E., 2007. Irreversibility and fluctuation theorem in stationary time series. *Physical Review Letters*, 98(9), 094101.

Prigogine, I. and Stengers, I., 1997. *The End of Certainty*. Simon and Schuster, New York.

Psaradakis, Z., 2008. Assessing time-reversibility under minimal assumptions. *Journal of Time Series Analysis*, *29*(5), pp.881-905.

Racine, J.S. and Maasoumi, E., 2007. A versatile and robust metric entropy test of time-reversibility, and other hypotheses. *Journal of Econometrics*, 138 (2), 547-567.

Ramsey, J.B., Rothman, P., 1996. Time irreversibility and business cycle asymmetry. *Journal of Money, Credit, and Banking* 28 (1), 1-21.

Soon, W., 2007. Implications of the secondary role of carbon dioxide and methane forcing in climate change: past, present, and future. *Physical Geography,* 28(2), 97-125.

Suppes, P., 1970. *A Probabilistic Theory of Causality*, North-Holland Publishing, Amsterdam.

Tong, H. and Zhang, Z., 2005. On time-reversibility of multivariate linear processes. *Statistica Sinica*, 15 (2), 495-504.

Tsoukalas I., Makropoulos C., and Koutsoyiannis D., 2018. Simulation of stochastic processes exhibiting any-range dependence and arbitrary marginal distributions, *Water Resources Research*, 54 (11), 9484-9513, doi: 10.1029/2017WR022462.

Weiss, G., 1975. Time-reversibility of linear stochastic processes. *Journal of Applied Probability*, 12(4), 831-836.